

Article

High Endemism in an Endangered Biodiversity Hotspot: Phylogeny, Taxonomy and Distribution Patterns of Catfishes of the *Psammocambeva* Alpha-Clade (Siluriformes: Trichomycteridae) from the Rio Doce Basin, Brazil

Wilson J. E. M. Costa ^{*}, José Leonardo O. Mattos , Maria Anaís Barbosa, Paulo J. Vilaro  and Axel M. Katz 

Laboratory of Systematics and Evolution of Teleost Fishes, Institute of Biology, Federal University of Rio de Janeiro, Rio de Janeiro CEP 21941-971, Brazil; jlomattos@gmail.com (J.L.O.M.); anaisbarbosasv@gmail.com (M.A.B.); kpaulojose@gmail.com (P.J.V.); axelmk@gmail.com (A.M.K.)

* Correspondence: wcosta@acd.ufrj.br

Abstract: The Rio Doce basin is situated in a biodiversity hotspot, with some fish groups still superficially known. The intense process of habitat loss and water contamination justifies efforts to speed up the pace of describing fish species diversity. Herein, we focus on a clade of trichomycterine catfishes, subgenus *Psammocambeva*, genus *Trichomycterus*, performing a multigene phylogenetic analysis, which integrated to a comparative morphological analysis corroborates monophyly and relationships of four species complexes. Five new species are recognised and described. Species distribution patterns support the recognition of five areas of endemism for trichomycterines, most of which are well-known biodiversity centres: Serra do Espinhaço, Serra do Brigadeiro, Serra do Caparaó, Serra do Castelo, and upper-middle Rio Doce. Trichomycterine diversity in the Rio Doce basin, with 16 species, of which 15 belong to *Psammocambeva*, is lower than in the smaller neighbouring Rio Paraíba do Sul basin, with 21 species in five subgenera. Data suggest that species diversification in the former basin is relatively younger, following the initial diversification of *Psammocambeva* in the Miocene, whereas diversification in the latter basin has been estimated to have occurred during the Oligocene. This study reinforces the importance of naming new taxa and delimitating areas of endemism as primary tools for conservation strategies.

Keywords: Atlantic Forest; comparative osteology; mountain biodiversity; multigene phylogeny; Serra do Brigadeiro; Serra do Caparaó; Serra do Castelo; Serra do Espinhaço

Key Contribution: This paper comprises the greatest genetic sample and the most complete taxon sample for the *Psammocambeva* alpha-clade; new osteological characters supporting species diagnoses and relationships; descriptions of five new species; and delineation of areas of endemism for mountain catfishes in the Rio Doce basin relative to well-known high biodiversity centres.



Citation: Costa, W.J.E.M.; Mattos, J.L.O.; Barbosa, M.A.; Vilaro, P.J.; Katz, A.M. High Endemism in an Endangered Biodiversity Hotspot: Phylogeny, Taxonomy and Distribution Patterns of Catfishes of the *Psammocambeva* Alpha-Clade (Siluriformes: Trichomycteridae) from the Rio Doce Basin, Brazil. *Fishes* **2023**, *8*, 474. <https://doi.org/10.3390/fishes8100474>

Academic Editor: Joseph Quattro

Received: 30 July 2023

Revised: 16 September 2023

Accepted: 19 September 2023

Published: 22 September 2023



Copyright: © 2023 by the authors. Licensee MDPI, Basel, Switzerland. This article is an open access article distributed under the terms and conditions of the Creative Commons Attribution (CC BY) license (<https://creativecommons.org/licenses/by/4.0/>).

1. Introduction

The Rio Doce basin (hereafter RDB), draining an area of about 86,700 km², has its main sources situated in two mountain ranges, the Serra do Espinhaço and the Serra da Mantiqueira, two of the largest biodiversity centres in South America [1,2]. Western and north-western headwaters drain the southern plateau of the Serra do Espinhaço, whereas south-western and southern headwaters drain the northern plateau of the Serra da Mantiqueira, which comprises separate nuclei such as the Serra do Brigadeiro, Serra do Caparaó, and Serra do Castelo. Each of these mountain range segments shelters a diversified biota with high rates of endemism for plants and some animal groups (see discussion below). However, knowledge about the ichthyofauna of RDB is still incomplete, with several species being described in recent years (e.g., [3–6]). On the other hand,

there are numerous mining enterprises in the region, besides an old and still intense deforestation process caused by livestock activities, endangering the rich biodiversity. The recent catastrophic environmental accident caused by the rupture of a mine tailings dam in the upper section of the basin resulted in serious damage to the local ichthyofauna, putting several species at imminent risk of extinction [7–9]. The great species diversity combined with accentuated environmental degradation justifies efforts to speed up the pace of formal descriptions of components of the local biota that are still little known.

Among the components of the fluvial vertebrate fauna of RDB, trichomycterine catfishes stand out as they comprise the most diverse group of fish in the fast-flowing river and streams of south-eastern Brazil [10]. In this region, trichomycterines are formally placed in the genus *Trichomycterus* Valenciennes, 1832 and are members of the clade highly supported by molecular data [11] and designated as *Trichomycterus sensu stricto* [10] (hereafter *Trichomycterus s.s.*). *Trichomycterus s.s.* includes the type species of the genus *Trichomycterus nigricans* Valenciennes, 1832, and about 50 other species from south-eastern and north-eastern Brazil, divided into six subgenera [10–13]. Among the subgenera of *Trichomycterus*, *Psammocambeva* Costa, 2021, the focus of the present study, has the largest geographical distribution, occurring in south-eastern and north-eastern Brazil [10,14]. Most species of *Psammocambeva* belong to the *Psammocambeva* alpha-clade (PAC), which typically includes species reaching about 60–100 mm of standard length (SL), often with a relatively large eye and a variably spotted colour pattern, besides a long maxillary bone that is longer than the premaxilla [10]. Although PAC is not diagnosable using unique morphological character states, it is strongly supported by molecular data [12,14].

The first species of PAC described from RDB was *Trichomycterus alternatus* (Eigenmann, 1917). Its description was based on 67 specimens collected near the village of Rio Doce by John Haseman in 1908 [15–17]. Over 100 years later, Reis et al. [18] described a second species of PAC, *Trichomycterus astromycterus* Reis, de Pinna and Pessali, 2019 from the same area as *T. alternatus*. Reis and de Pinna [6] revised trichomycterine species from RDB, describing a third species of PAC, *Trichomycterus vinnulus* Reis and de Pinna, 2022, from that same area as those two species previously described.

Reis and de Pinna [6] considered *T. alternatus* to be a geographically widespread metaspecies, occurring in other river basins of south-eastern Brazil. Two species from the Rio Paraíba do Sul basin, *Trichomycterus auroguttatus* Costa, 1992, and *Trichomycterus travassosi* (P. Miranda-Ribeiro, 1949), were then considered to be synonyms of *T. alternatus*. Subsequently, Costa et al. [12] revised species of PAC from a region comprising the Rio Paraíba do Sul basin and adjacent smaller coastal basins based on a multigene phylogeny (i.e., two mitochondrial and two nuclear genes, total of 2974 bp) and morphological characters. In this paper, the authors recognised eight valid species of PAC to be endemic to that region, including *T. auroguttatus* and *T. travassosi*. In addition, Costa et al. [12] provided phylogenetic evidence that species of PAC belong to four species complexes, but several nodes of the phylogenetic tree were weakly supported.

Costa et al. [12] listed three nominal species of PAC endemic to RDB: *T. alternatus*, *T. astromycterus*, and *T. vinnulus*, all from the same area, occurring in streams close to the main course of the upper-middle section of the Rio Doce. However, our field collections between 2002 and the present in different parts of RDB have indicated the occurrence of some still undescribed species of PAC. We herein perform a new multigene phylogeny with a broader genetic sample (3665 bp) for all species of PAC, describe five new species, and discuss the distribution patterns of PAC in RDB.

2. Materials and Methods

2.1. Specimens

Collections were made with dip nets during daylight. This study included both specimens already deposited in the fish collection during the last two decades and specimens from recent collections specifically focused on trichomycterines from the Rio Doce basin, using collecting permits given by ICMBio (Instituto Chico Mendes de Conservação

da Biodiversidade; permit number: 38553-13). Field methods, including euthanasia that followed the AVMA Guidelines for the Euthanasia of Animals [19], were approved by CEUA-CCS-UFRJ (Ethics Committee for Animal Use of Federal University of Rio de Janeiro; permit number: 065/18). Specimens were fixed just after collection in formalin; two weeks after, they were transferred to 70% ethanol, where they were preserved. Some specimens were fixed and preserved in absolute ethanol, which is more amenable to subsequent DNA extraction. Osteological preparations followed [20]; specimens so prepared are indicated in lists by C&S (=cleared and stained) and are preserved in glycerine. Specimens were deposited in the ichthyological collections of Instituto de Biologia, Universidade Federal do Rio de Janeiro (UFRJ) and Centro de Ciências Agrárias e Ambientais, Universidade Federal do Maranhão (CICCAA).

In order to include topotype specimens of *T. alternatus* in the analysis, two of us (AMK and PJV) made three collecting trips (July 2021, September 2022, and May 2023) to the region around the village of Rio Doce, upper Rio Doce basin, type locality region of *T. alternatus*. However, only one small specimen was found, UFRJ 13165, 1 ex., 30.7 mm standard length (SL) (cleared and stained; collected at 20°11'40" S 42°51'09" W), likely a result of the great recent, catastrophic environmental impacts in this area. This region was drastically affected by the flood of tailings from the 2015 disaster in Mariana that blocked the dam of the Risoleta Neves Hydroelectric Plant. Some works for channelling tributaries of the Rio Doce in this area were carried out in more recent years, a process that may have been decisive for the near extinction of *T. alternatus* in the type locality area. This specimen exhibited external morphological traits like in specimens of the type series of *T. alternatus* and topotypes (e.g., figure 2 in Ref. [6]), as well as osteological meristic data as in type specimens. Data on type specimens of *T. alternatus* were obtained from photos of holotype (FMNH 58082) and radiographs of the holotype and 67 paratypes (FMNH 58083) deposited in the Fish Collection of the Field Museum of Natural History (https://collections-zoology.fieldmuseum.org/list?f%5B0%5D=ss_CatCatalog%3A%22Fishes%22; last access on 25 July 2023). Geographical names cited in specimen lists are according to Portuguese names used in the region. A complete list of comparative material appears in Costa et al. [12].

2.2. Morphological Data

Measurements followed Costa [21], with modifications described in Costa et al. [22] and were presented as percent of standard length (SL) or head length. Only well-preserved specimens, fixed in formalin, with 40 mm SL or more were measured. Fin ray formulae followed Costa et al. [21], using standards described in Bockmann and Sazima [23]. All vertebra elements, except the Apparatus of Weber, were included in counts. Osteological illustrations were prepared using drafts of dissected C&S specimens made with a Zeiss Stemi SV 6 stereomicroscope fitted with a camera lucida. Terminology for osteological structures follows Costa [10], except for using lacrimal instead of antorbital, following Kubicek [24]. Osteological descriptions focused on structures with informative taxonomic variation among species of PAC [12]. Terminology for pores of the latero-sensory system followed Arratia and Huaquin [25], with modifications proposed by Bockmann and Sazima [23]. In order to compare species colour patterns using equivalent homologous distribution of dark chromatophores in body zones, four longitudinal dark pigmentation zones (LDPZ) were identified and consistently used in species description (Figure 1): LDPZ 1: on the longitudinal midline of the dorsum, between the nape and the posterior portion of the caudal peduncle; LDPZ 2: on the dorsal portion of the flank, between the nape and the posterior portion of the caudal peduncle; LDPZ 3: on the longitudinal midline of the flank, between the humeral region and the posterior portion of the caudal peduncle; LDPZ 4: on the ventral portion of the flank, between the area at a vertical through the pelvic-fin base and the posterior portion of the caudal peduncle.

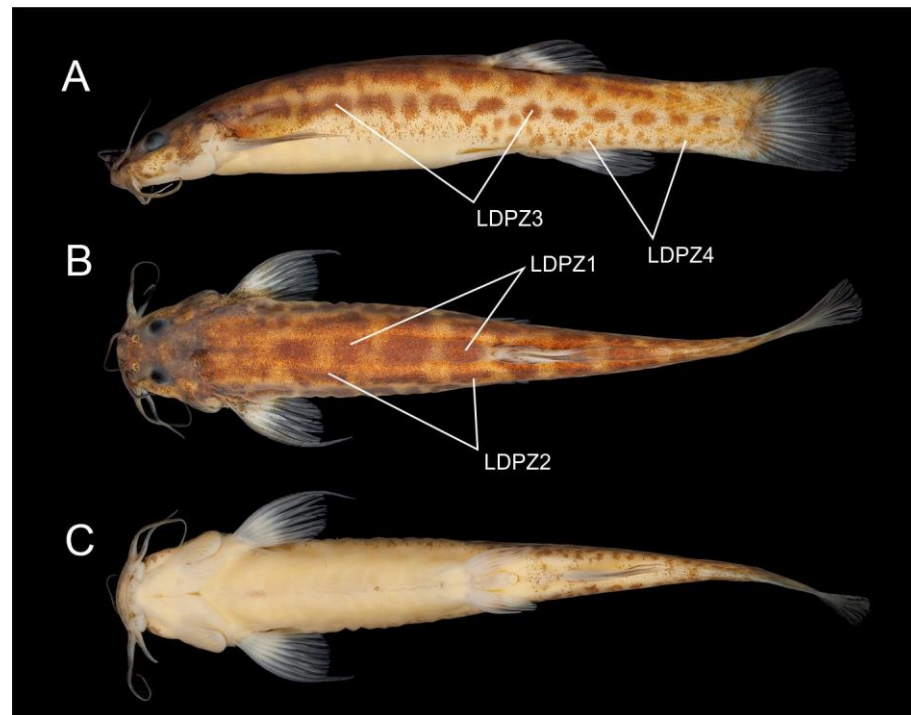


Figure 1. *Trichomcyterus* sp. aff. *T. goeldii*, UFRJ 13107, Serro Municipality, 43.1 mm SL: (A) lateral, (B) dorsal, and (C) ventral views.

2.3. DNA Extraction, Amplification and Sequencing

Small pieces of muscle tissue were removed from the right side of the caudal peduncle for DNA extraction using DNeasy Blood and Tissue Kit (Qiagen, Hilden, NRM, Germany). Agarose gel electrophoresis was employed to check the quality of the DNA extraction product. The polymerase chain reaction (PCR) was performed using the following primers: Cytb Siluri F and Cytb Siluri R [26] for *cytochrome b* (CYTB); FISH-F1 and FISH-R1 [27] for *cytochrome c oxidase I* (COX1); and H3 L11935 and H12857 [28] for NADH: *ubiquinone oxidoreductase core subunit 4* (ND4); RAG2 TRICHO F and RAG2 TRICHO R [29] for the *recombination activating 2* (RAG2); MYH6 TRICHO F and MYH6 TRICHO R [29] for the *myosin heavy chain 6* (MYH6). Parameters for PCR reactions carried out in 45 μ L were as follows: 5 \times GreenGoTaq Reaction Buffer (Promega, Madison, WI, USA), 1.0 mM MgCl₂, 0.5 μ M of each primer, 0.2 mM of each dNTP, 1 u of Promega GoTaq Hot Start polymerase and 50 ng of genomic DNA. Negative controls to check for contaminants were applied to all reactions. The following PCR thermal profile protocol was used: denaturation for 5 min at 95 $^{\circ}$ C, 35 cycles of denaturation for 1 min at 94 $^{\circ}$ C, and annealing for 1 min. at 50–60 $^{\circ}$ C and extension for 1–1.5 min at 72 $^{\circ}$ C; and final extension for 7 min at 72 $^{\circ}$ C. PCR product purification was made using the Wizard SV Gel and PCR Clean-Up System (Promega). Sequencing reactions were made with the BigDye Terminator Cycle Sequencing Mix (Applied Biosystems, Waltham, MA, USA). The sequencing reaction thermal profile, performed in 20 μ L reaction volumes containing 4 μ L BigDye, 2 μ L sequencing buffer 5 \times (Applied Biosystems), 2 μ L of the PCR products (30–40 ng), 2 μ L primer and 10 μ L deionised water, was the following: 35 cycles of 10 s at 96 $^{\circ}$ C, 5 s at 54 $^{\circ}$ C and 4 min at 60 $^{\circ}$ C. MEGA 11 [30] was used for reading and interpreting chromatograms, as well as to translate sequences into amino acid residues to verify the codification of each gene sequence and the absence of premature stop codons or indels. GenBank accession numbers are provided in Appendix A.

2.4. Phylogenetic Analysis

Terminal taxa comprised 22 terminal taxa, which represented all species of PAC, including the five new species. Outgroups comprised three species of *Psammocambeva* representing other subgeneric lineages, four species of *Trichomycterus* representing other subgenera, two species representing the clade comprising *Cambeva* Katz, Barbosa, Mattos and Costa, 2018 plus *Scleronema* Eigenmann, 1917, the sister group of *Trichomycterus* [12]; one trichomycterine species representing another subfamilial lineage; two species representing other trichomycterid subfamilies; and one nematogenyid species, a basal representative of loricarioid catfishes. Separate gene datasets (COX1 521 bp, CYTB 1088 bp, RAG2 821 bp, ND4 692 bp, MYH6 543 bp) were aligned using the Clustal W algorithm [31] implemented in MEGA 11. No gaps or stop codons were found. The PartitionFinder 2.1.1 (Canberra, ACT, Australia) [32] algorithm was used to calculate the optimal partition scheme and best-fit evolutive models based on the Corrected Akaike Information Criterion (Appendix B). Two independent approaches for phylogenetic reconstruction were performed for the concatenated molecular data matrix (3665 bp): Bayesian Inference, using MrBayes 3.2.7a [33] (two independent Markov chain Monte Carlo (MCMC) runs with 5×10^7 generations, with a sampling frequency of every 1000 generations; convergence of the MCMC chains, attainment of the stationary phase, effective sample size adequacy, and determination of the burn-in percentage evaluated using Tracer 1.7.2 (Auckland, Auckland Region, New Zealand) [34]; and the majority-rule consensus of saved trees and Bayesian posterior probabilities calculated applying a 25% burn-in) and Maximum Likelihood, using GARLI 2.0 (Lawrence, KS, USA) [35], with branch support assessed using the values of the majority-rule consensus tree calculated with 1000 nonparametric bootstrap replicates [36].

3. Results

3.1. The *Psammocambeva* Alpha-Clade

Both phylogenetic analyses generated identical trees (Figure 2). PAC and all species complexes proposed by Costa et al. [12] were corroborated, and node support was high for PAC and for most internal nodes. As in the previous study, PAC is supported as a sister to *Trichomycterus longibarbatius* Costa, 1992. Species of PAC share a robust opercular odontode patch (Figure 3), a condition not occurring in *T. longibarbatius* (figure 4B in Ref. [12]) and most species of the CST-clade, but present in some other species of *Trichomycterus* [10]. The following morphological description is applicable to all species of PAC.

General morphology: Body moderately slender, weakly depressed anteriorly, compressed posteriorly. Dorsal and ventral profiles of the head and trunk are slightly convex, about straight on the caudal peduncle. Greatest body depth at vertical immediately anterior to pelvic-fin base. Head sub-trapezoidal in dorsal view, anterior profile of snout slightly convex. The eye is positioned on the dorsal portion of the head. Anterior and posterior nostrils in close proximity, the distance between them smaller than the distance between the posterior nostril and orbital rim. Mouth subterminal. The pectoral fin is subtriangular, and the anterior and posterior margins are slightly convex. First, the pectoral-fin ray is long, surpassing the fin membrane to form a free filament. Pelvic fin narrow and rounded, posteriorly surpassing urogenital papilla.

Laterosensory system: Supraorbital canal continuous, with three pores: s1, adjacent to the medial margin of anterior nostril; s3, adjacent and just posterior to the medial margin of posterior nostril; s6, at the transverse line through posterior margin of orbit. The infraorbital sensory canal is represented by two separate sections. Anterior infraorbital section, when present isolated, attached to lacrimal, with two pores: i1, at the transverse line through the anterior nostril, i3, at the transverse line just anterior to the posterior nostril. The posterior infraorbital section is posteriorly connected to supraorbital and postorbital canals, with two pores: i10, adjacent to the ventral margin of the orbit, and i11, posterior to the orbit. Postorbital canal with two pores: po1, at the vertical line above the posterior portion of an interopercular patch of odontodes, po2, at the vertical line above the posterior portion of

an opercular patch of odontodes. The lateral line of the body is short, with two pores just posterior to the head.

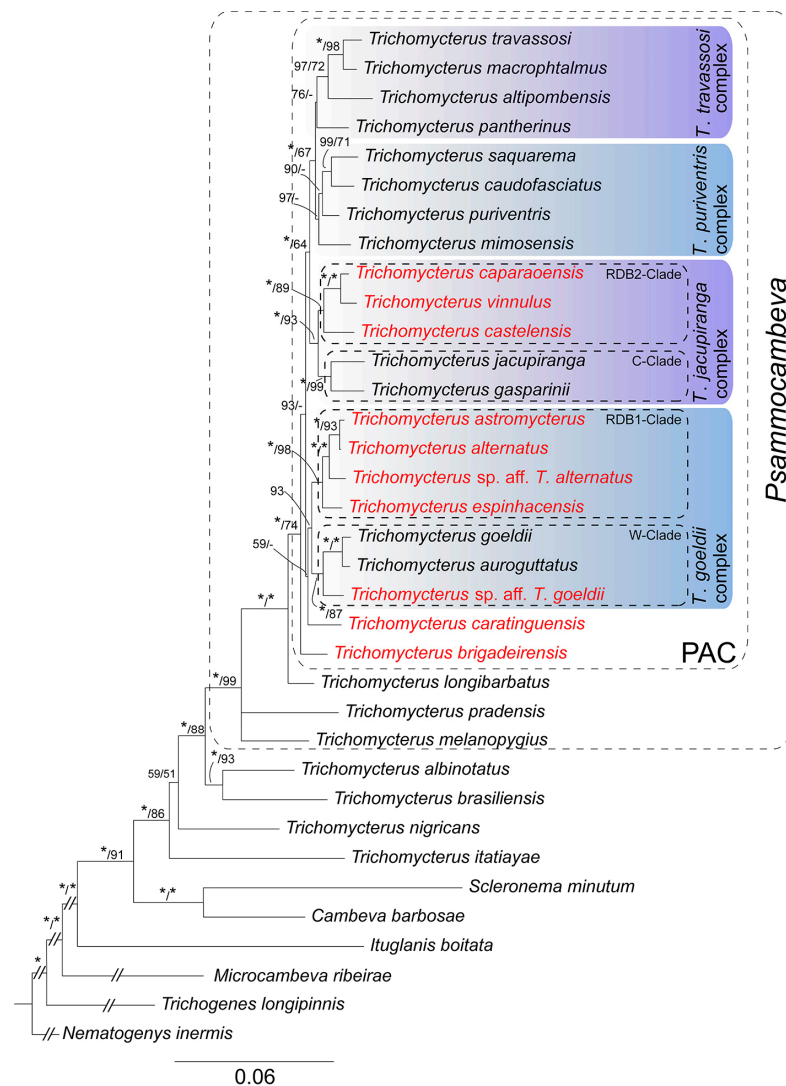


Figure 2. Bayesian Inference tree estimated by MrBayes 3.2.7a for 29 species of *Trichomycterus* and six outgroup taxa; data set comprises three mitochondrial encoded genes and two nuclear genes (COI, CYTB, ND4, RAG2 and MYH6), a total of 3665 bp. The numbers above branches indicate Bayesian posterior probabilities of the Bayesian Inference analysis and the bootstrap values of the Maximum Likelihood analyses, respectively, separated by a bar. Asterisks (*) indicate maximum support values, and dashes (-) indicate values below 50. Red taxa are species of PAC endemic to the Rio Doce basin.

3.2. Relationships and Taxonomy of Main PAC Lineages

The phylogenetic analyses supported species of PAC from RDB belonging to four lineages (Figure 2): 1—*Trichomycterus brigadeirensis* Costa, Katz and Vilar do sp. nov., from the Serra do Brigadeiro and below described, supported as sister to a clade comprising all other species of PAC; 2—*Trichomycterus caratinguensis* Costa, Katz and Vilar do sp. nov., from the Rio Caratinga drainage and below described, weakly supported as sister to the *T. goeldii* complex; 3—the *Trichomycterus goeldii* complex as delimited in Costa et al. [12]; 4—the *Trichomycterus jacupiranga* as delimited in Costa et al. [12]. No species from RDB belong to the *Trichomycterus puriventris* and *Trichomycterus travassosi* complexes.

Trichomycterus brigadeirensis Costa, Katz and Vilar do sp. nov.

LSID:urn:lsid:zoobank.org:act:4E1ADC38-014E-4A3F-B8DE-AD09935F3996

Figures 3A, 4, 5A, 6A and 7A; Table 1

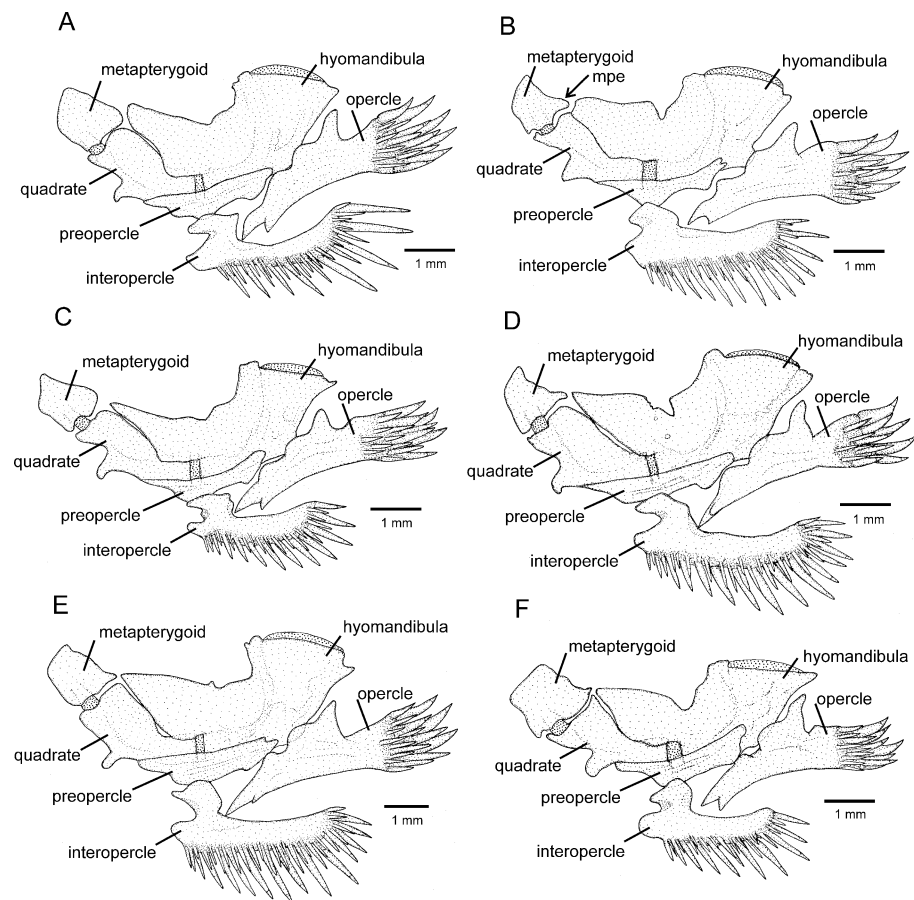


Figure 3. Left jaw suspensorium and opercular series, lateral view: (A) *Trichomycterus brigadeirensis* Costa, Katz and Vilardo sp. nov.; (B) *Trichomycterus caratinguensis* Costa, Katz and Vilardo sp. nov.; (C) *Trichomycterus espinhacensis* Costa and Katz sp. nov.; (D) *Trichomycterus caparaoensis* Costa, Barbosa and Katz sp. nov.; (E) *Trichomycterus castelensis* Costa, Katz and Vilardo sp. nov.; (F) *Trichomycterus vinnulus*. mpe: metapterygoid posterior extension. Larger stippling represents cartilage.

Holotype. UFRJ 13480, 78.6 mm SL; Brazil: Minas Gerais State: Araponga Municipality: Ribeirão Félix, upper Rio Casca drainage, Rio Doce basin, Serra do Brigadeiro, 20°41'31" S 42°29'52" W, altitude about 1,100 m; A. M. Katz and P. J. Vilardo, 25 September 2022.

Paratypes. UFRJ 13239, 10 ex., 26.8–65.7 mm SL; UFRJ 13655, 4 ex. (C&S), 33.1–47.1 mm SL; UFRJ 13169, 4 ex. (DNA), 30.3–36.0 mm SL; CICC AA 07772, 2 ex., 45.1–45.8 mm SL; all collected with holotype.

Diagnosis. *Trichomycterus brigadeirensis* differs from all other congeners of PAC using the following unique combination of character states: 19–21 dorsal procurrent caudal-fin rays (vs. 13–15 in *Trichomycterus saquarema* Costa, Katz, Vilardo, and Amorim, 2022; 16–18 in *T. auroguttatus*, *Trichomycterus caudofasciatus* Alencar and Costa, 2004, *Trichomycterus goeldii* Boulenger, 1896, *T. mimosensis* Barbosa, 2013, and *T. vinnulus*; and 22–28 in *Trichomycterus altipombensis* Costa, Katz, Vilardo, and Mattos, 2022, *T. astromycterus*, *Trichomycterus espinhacensis* Costa and Katz sp. nov., *Trichomycterus macrophthalmus* Barbosa and Costa, 2012, and *T. travassosi*); 14–16 ventral procurrent caudal-fin rays (vs. 8–13 in *T. altipombensis*, *T. astromycterus*, *T. auroguttatus*, *T. goeldii*, *Trichomycterus jacupiranga* Wosiacki and Oyakawa, 2005, *T. saquarema*, *T. travassosi*, and *T. vinnulus*); 28–33 premaxillary teeth (vs. 39–60 in *T. auroguttatus*, *Trichomycterus caratinguensis* Costa, Katz, and Vilardo sp. nov., *Trichomycterus castelensis* Costa, Katz, and Vilardo sp. nov., *T. goeldii*, *T. macrophthalmus*, *T. mimosensis*, *Trichomycterus purivoentris* Barbosa, and Costa, 2012, *T. saquarema*, and *T. vinnulus*); 8 pectoral-fin rays (vs. 7 in *Trichomycterus gasparinii* Barbosa, 2013 and *T. pantherinus*); 36–38 vertebrae (vs. 33–35 in *T. astromycterus*, *T. jacupiranga*, *T. mimosensis*, and *T. travassosi*); 12–13 ribs

(vs. 10–11 in *T. alternatus*, *T. altipombensis*, *T. astromycterus*, *T. auroguttatus*, *T. caudofasciatus*, *T. espinhacensis* Costa and Katz sp. nov., *T. jacupiranga*, *T. macrophthalmus*, *T. travassosi*, and *T. vinnulus*; and 14 in *T. caratinguensis* Costa, Katz, and Vilaro sp. nov.); the dorsal-fin origin at a vertical between the centrum of the 18th and 20th vertebra (vs. between the centrum of the 16th and 17th vertebra in *T. altipombensis*, *T. auroguttatus*, *T. caratinguensis* Costa, Katz, and Vilaro sp. nov., *T. caudofasciatus*, *T. espinhacensis* Costa and Katz sp. nov., *T. macrophthalmus*, and *T. travassosi*, and between the centrum of the 14th and 15th vertebra in *T. astromycterus*); pointed mandibular teeth (vs. incisor-like in *T. astromycterus* and *T. jacupiranga*); the presence of the anterior segment of the infraorbital series (vs. absence in *T. gasparinii* and *T. pantherinus*); and presence of a broad dark brown stripe between the humeral region and the caudal-fin base (vs. absence in *T. alternatus*, *T. altipombensis*, *T. astromycterus*, *T. auroguttatus*, *T. caudofasciatus*, *T. espinhacensis* Costa and Katz sp. nov., *T. gasparinii*, *T. goeldii*, *T. macrophthalmus*, *T. mimosensis*, *T. travassosi*, and *T. vinnulus*). *Trichomycterus brigadeirensis* may also be distinguished from all other species of PAC using its colour pattern, in which LDPZ 1 and 2 are represented using brown round spots longitudinally in close proximity, weakly distinguishable from colour ground (vs. LDPZ 1 and 2 marks highly contrasting with lighter colour ground).



Figure 4. *Trichomycterus brigadeirensis* Costa, Katz and Vilaro sp. nov. Holotype, UFRJ 13480, Araponga, 78.6 mm SL: (A) lateral, (B) dorsal, and (C) ventral views.

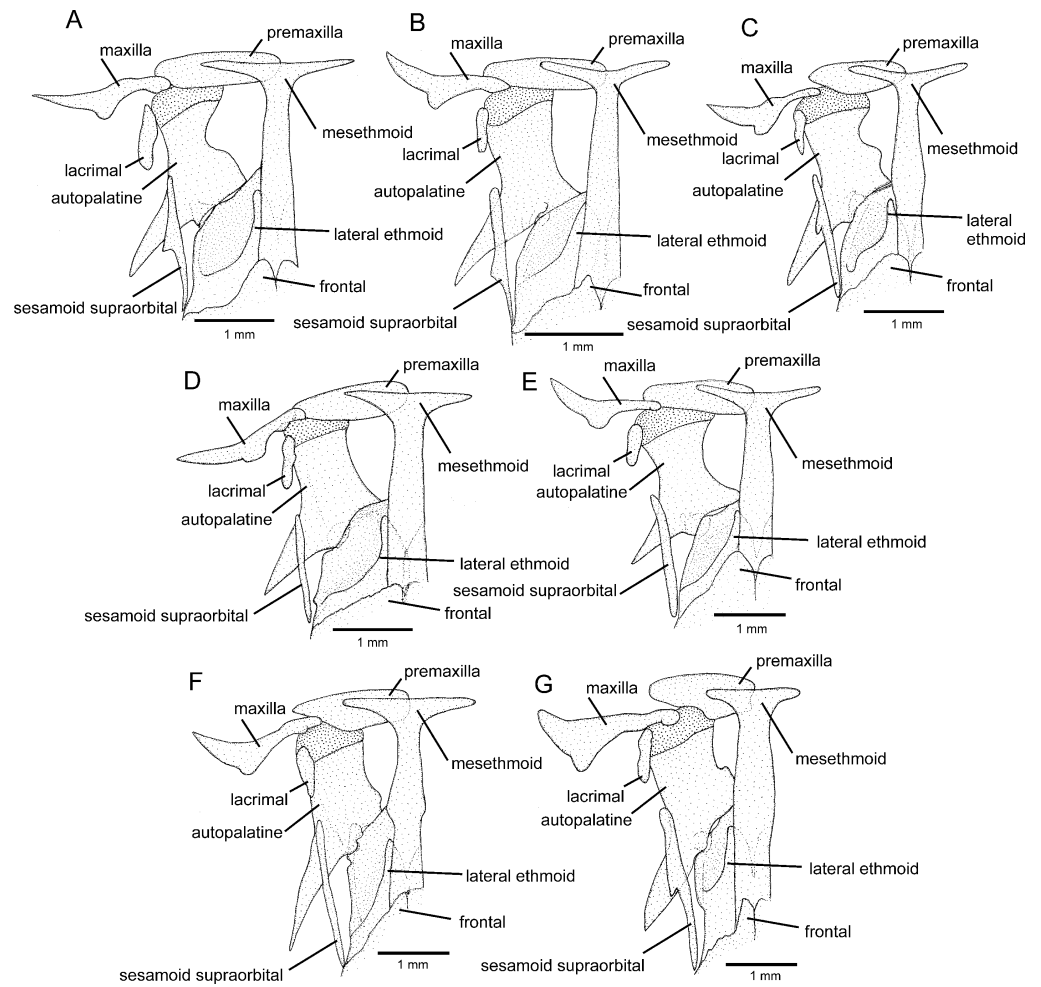


Figure 5. Mesethmoidal region, middle and left portions, dorsal view: (A) *Trichomycterus brigadeirensis* Costa, Katz and Vilardo sp. nov.; (B) *Trichomycterus caratinguensis* Costa, Katz and Vilardo sp. nov.; (C) *Trichomycterus espinhacensis* Costa and Katz sp. nov.; (D) *Trichomycterus caparaoensis* Costa, Barbosa and Katz sp. nov.; (E) *Trichomycterus castelensis* Costa, Katz and Vilardo sp. nov.; (F) *Trichomycterus vinnulus*; (G) *Trichomycterus astromycterus*. Larger stippling represents cartilage.

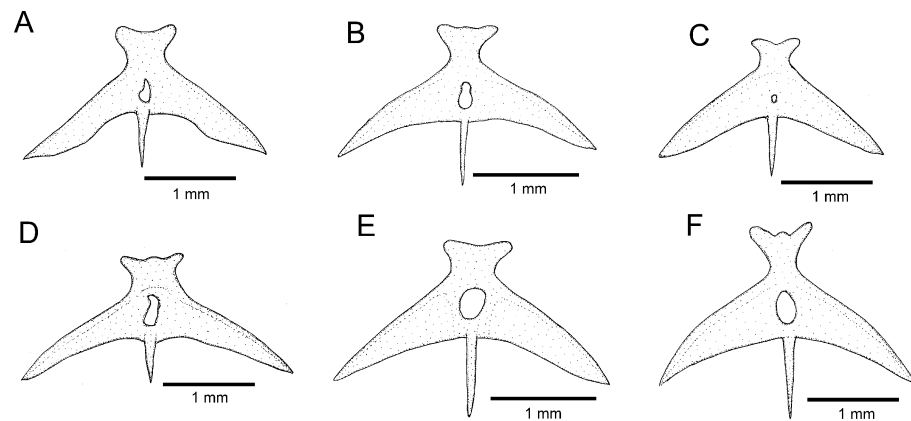


Figure 6. Parurohyal, ventral view: (A) *Trichomycterus brigadeirensis* Costa, Katz and Vilardo sp. nov.; (B) *Trichomycterus caratinguensis* Costa, Katz and Vilardo sp. nov.; (C) *Trichomycterus espinhacensis* Costa and Katz sp. nov.; (D) *Trichomycterus caparaoensis* Costa, Barbosa and Katz sp. nov.; (E) *Trichomycterus castelensis* Costa, Katz and Vilardo sp. nov.; (F) *Trichomycterus vinnulus*.

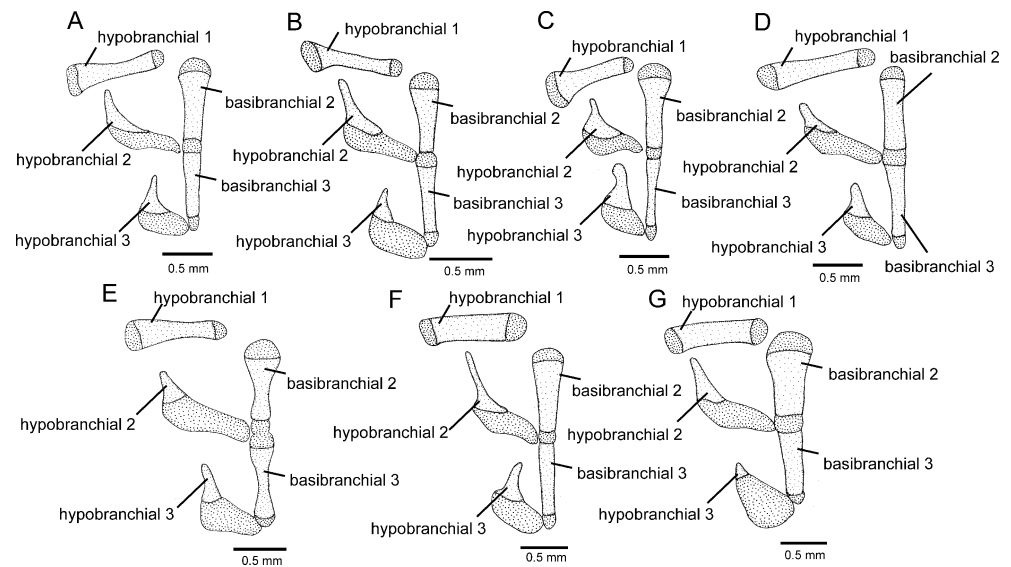


Figure 7. Ventral branchial skeleton, middle and left portions, dorsal view: (A) *Trichomycterus brigadeirensis* Costa, Katz and Vilardo sp. nov.; (B) *Trichomycterus caratinguensis* Costa, Katz and Vilardo sp. nov.; (C) *Trichomycterus espinhacensis* Costa and Katz sp. nov.; (D) *Trichomycterus caparaensis* Costa, Barbosa and Katz sp. nov.; (E) *Trichomycterus castelensis* Costa, Katz and Vilardo sp. nov.; (F) *Trichomycterus vinnulus*; (G) *Trichomycterus astromycterus*. Larger stippling represents cartilage.

Table 1. Morphometric data of *Trichomycterus brigadeirensis* Costa, Katz and Vilardo sp. nov.

	Holotype	Paratypes (n = 10)
Standard length (SL)	78.6	37.3–65.7
Percentage of standard length		
Body depth	15.6	14.6–18.3
Caudal peduncle depth	11.6	10.6–11.9
Body width	12.8	11.3–13.8
Caudal peduncle width	4.0	2.9–4.8
Pre-dorsal length	62.5	57.2–66.0
Pre-pelvic length	56.5	55.7–60.0
Dorsal-fin base length	10.4	10.2–13.1
Anal-fin base length	8.4	7.9–12.1
Caudal-fin length	17.0	15.3–19.9
Pectoral-fin length	14.7	13.7–17.4
Pelvic-fin length	12.1	10.1–14.0
Head length	19.4	19.4–22.5
Percentage of head length		
Head depth	51.0	46.6–56.8
Head width	91.8	83.4–94.4
Snout length	39.5	10.9–46.3
Interorbital width	26.6	25.6–31.0
Preorbital length	12.5	10.3–13.3
Eye diameter	12.5	12.5–19.5

Description. General morphology: Morphometric data are in Table 1. The dorsal surface of the head is plain between orbits, the eye slightly projected dorsally. Maxillary barbel posteriorly reaching pectoral-fin base, rictal barbel reaching between the middle and posterior portion of an interopercular patch of odontodes, nasal barbel reaching the area just anterior to opercle or barely touching it. Jaw teeth pointed. Premaxillary teeth 28–33, slightly curved, arranged in irregular rows. Dentary teeth 32–39, slightly curved backwards, irregularly arranged. Opercular odontodes 13–17, interopercular odontodes 35–37. Odontodes pointed, arranged in irregular rows. Anterior infraorbital canal present.

Single median s6. Dorsal and anal fins are subtriangular, anterior margin straight, posterior margin slightly convex. Total dorsal-fin rays 12 (iii + II + 7), total anal-fin rays 9 or 10 (ii–iii + II + 5). Anal-fin origin at vertical through posterior portion of dorsal-fin base, at base of 6th bifid dorsal-fin ray. Pectoral-fin filament length is about 25–40% of pectoral-fin length without filament. Total pectoral-fin rays 8 (I + 7). Pelvic fin posteriorly reaching vertical just posterior to middle dorsal-fin base. Pelvic-fin bases are medially separated by interspace about three-fourths pelvic-fin base. Total pelvic-fin rays 5 (I + 4). Caudal fin sub-truncate, upper and lower corners rounded. Total principal caudal-fin rays 13 (I + 11 + I), total dorsal procurent rays 19–21 (xviii–xx + I), total ventral procurent rays 14–16 (xiii–xv + I). Anus and urogenital papilla at vertical through area just anterior to middle of dorsal-fin base.

Osteology (Figures 3A, 5A, 6A and 7A): Anterior margin of mesethmoid slightly concave, mesethmoid cornu rod-shaped. Lacrimal broad and flat, nearly elliptical; sesamoid supraorbital narrow and flat, with lateral expansion; sesamoid supraorbital length about two times lacrimal length. The premaxilla is sub-rectangular in the dorsal view. Maxilla boomerang-shaped, slender, slightly longer than premaxilla, with minute anterior expansion on subproximal region, posterior process well-developed. Autopalatine sub-rectangular in dorsal view when excluding posterolateral process, with pronounced lateral constriction posteriorly followed by weak sinuosity, shortest width about one-third of autopalatine length, lateral margin slightly convex. The postero-lateral process of autopalatine is subtriangular and long; its length is about three-fourths of autopalatine length. Metapterygoid subtrapezoidal, slightly deeper than long. Quadrate robust, dorso-posterior outgrowth in separated by minute interspace from hyomandibular outgrowth. Hyomandibula long, anterior outgrow shallow. The opercle is moderately elongated, the depth of the opercular odontode patch about four-fifths of the dorsal articular facet of the hyomandibula, and the dorsal process of the opercle is short and blunt. Interopercle long, about four-fifths of hyomandibula length. Preopercle compact, without ventral expansion. Basibranchials 2 and 3 elongate without distinctive constrictions; basibranchial 2 is an anterior region slightly wider than the posterior one, and basibranchial is rod-shaped. Hypobranchial 1 is a long, distal extremity slightly broader than the proximal extremity. Hypobranchials 2 and 3 are subtriangular, about equal in length; the basibranchial 2 is anterolaterally directed; the basibranchial 3 is anteriorly directed. Parurohyal robust, lateral process relatively elongate, pointed; parurohyal head well-developed, with prominent anterolateral paired process; middle foramen elliptical; posterior process short, about half length of distance between anterior margin of parurohyal and anterior insertion of posterior process. Branchiostegal rays 6 or 7. Vertebrae 36–38. Ribs 12–13. Dorsal-fin origin at vertical between centrum of 18th and 20th vertebra; anal-fin origin at vertical between centrum of 22nd and 23rd vertebra. Two dorsal hypural plates, corresponding to hypurals 4 + 5 and 3, respectively; single ventral hypural plate corresponding to hypurals 1 and 2 and parhypural.

Colouration in alcohol (Figure 4): The ground colour of the dorsum, dorsal portion of flank and head side is yellowish brown, becoming lighter on the ventral part of flank and head side. LDPZ 1 and 2 are represented by brown round spots longitudinally in close proximity, weakly distinguishable from colour ground. Dark brown chromatophores concentrated on a vertical zone on the posterior-most part of the caudal peduncle. LDPZ 3 is represented by a broad dark brown stripe between the humeral region and caudal-fin base, sometimes with short interruptions on its posterior portion. LDPZ 4 is represented by dark brown melanophores more concentrated on the posterior half of the flank, often coalesced, forming irregularly shaped marks. The dorsal and lateral surfaces of the head have a great concentration of dark brown spots, making it difficult to delimitate infraorbital, interopercular, and supraopercular marks. Venter white. Nasal barbel dark brown, maxillary and rictal barbels light grey. Fins hyaline, with small black spots on the basal portion of the pectoral and unpaired fins. In specimens below about 40 mm SL, LDPZ 1–4 are represented by small black spots, and LDPZ 3 often forms a narrow black longitudinal line.

Colouration in life: Similar to colouration in alcohol.

Distribution and habitat. *Trichomycterus brigadeirensis* is known only from the type locality, the Ribeirão Félix, a fast-flowing stream in the upper Rio Casca drainage, Rio Doce basin, Serra do Brigadeiro, southeastern Brazil (Figure 8). Specimens were collected at an altitude of about 1100 m, where the Ribeirão Félix is about 1.5–3.0 m wide and about 0.3–1.2 m deep, with clear water, bottom comprising sand and small pebbles about 10–15 cm of diameter, and secondary vegetation on stream margins. Specimens were found under small pebbles.

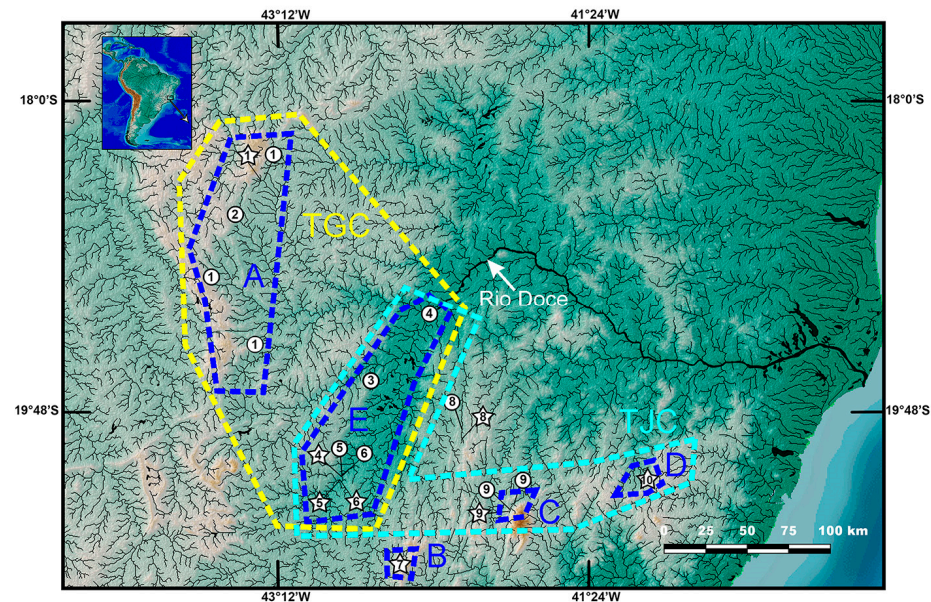


Figure 8. Geographical distribution of the *Psammocambeva* alpha-clade in the Rio Doce basin. 1, *Trichomycterus espinhacensis* Costa and Katz sp. Nov.; 2, *Trichomycterus* sp. Aff. *T. goeldii*; 3, *Trichomycterus* sp. Aff. *T. alternatus*; 4, *Trichomycterus astromycterus*; 5, *Trichomycterus alternatus*; 6, *Trichomycterus vinnulus*; 7, *Trichomycterus brigadeirensis* Costa, Katz and Vilardo sp. Nov.; 8, *Trichomycterus caratinguensis* Costa, Katz and Vilardo sp. Nov.; 9, *Trichomycterus caparaoensis* Costa, Barbosa and Katz sp. Nov.; 10, *Trichomycterus castelensis* Costa, Katz and Vilardo sp. Nov. Stars indicate type localities. A–E: areas of endemism; TGC: distribution of the *Trichomycterus goeldii* complex; TJC: *Trichomycterus jacupiranga* complex.

Etymology. The name *brigadeirensis* refers to the occurrence of the new species in the Serra do Brigadeiro.

3.3. The Clade *Trichomycterus caratinguensis* Costa, Katz and Vilardo sp. nov. plus the *T. goeldii* Complex

A clade comprising *T. caratinguensis* Costa, Katz and Vilardo sp. nov. and the *T. goeldii* complex was weakly supported in phylogenetic analyses (Figure 2) and not supported by any unique morphological character state. Therefore, the phylogenetic position of that new species is uncertain. The presence of a dark brown stripe between the humeral region and the caudal-fin base in *T. caratinguensis* Costa, Katz and Vilardo sp. nov. (Figure 9) and in both *T. brigadeirensis* (Figure 4), another species with basal phylogenetic position in PAC, would suggest that these species may be closest relatives. However, support values for the clade, including *T. caratinguensis* Costa, Katz and Vilardo sp. Nov. and all other species of PAC except *T. brigadeirensis* are high (Figure 2), thus making the hypothesis of these two species being sister taxa improbable. On the other hand, *T. caratinguensis* Costa, Katz and Vilardo sp. nov. possesses a small posterior expansion in the metapterygoid (Figure 3B), a condition considered diagnostic for a clade including all species of PAC except those belonging to the *T. goeldii* complex [12]. Therefore, although a similar expansion may occur in other generic trichomycterine lineages, making polarization of this character uncertain, the hypothesis of *T. caratinguensis* Costa, Katz and Vilardo sp. nov. to be sister to the

well-supported clade comprising the *T. jacupiranga*, *T. puriventris*, and *T. travassosi* complex cannot be discarded.

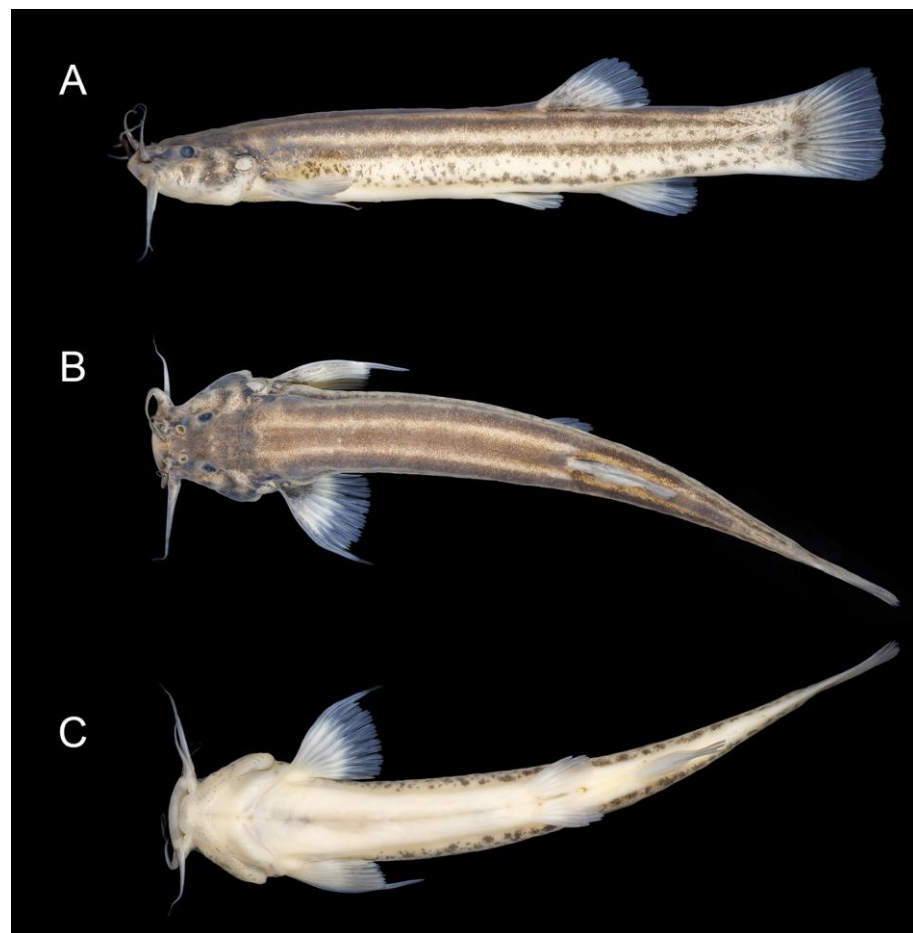


Figure 9. *Trichomycterus caratinguensis* Costa, Katz and Vilar do sp. nov. Holotype, UFRJ 13815, Santa Bárbara do Leste, 55.3 mm SL: (A) lateral, (B) dorsal, and (C) ventral views.

Trichomycterus caratinguensis Costa, Katz and Vilar do sp. nov.

LSID:urn:lsid:zoobank.org:act:CC19E25F-4730-4342-9413-26BEE380A23E

Figures 3B, 5B, 6B, 7B and 9; Table 2

Trichomycterus alternatus non *T. alternatus* (Eigenmann, 1917): figure 3H and 4A–C in Ref. [6]: (misidentification).

Holotype. UFRJ 13815, 55.3 mm SL; Brazil: Minas Gerais State: Santa Bárbara do Leste Municipality: Córrego Tabuleiro II, a tributary of Rio Caratinga, Rio Doce basin, 19°55'53" S 42°08'27" W, about 680 m asl; A. M. Katz and P. J. Vilar do, 19 May 2023.

Paratypes. All from Brazil: Minas Gerais State: Córrego Tabuleiro II, a tributary of Rio Caratinga, Rio Doce basin. Santa Bárbara do Leste Municipality: UFRJ 13816, 3 ex., 30.7–40.6 mm SL (C&S); UFRJ 13817, 4 ex., 23.4–28.9 mm SL; collected with holotype. Santa Rita de Minas Municipality: UFRJ 13238, 11 ex., 26.5–33.7 mm SL; CICC AA 07773, 4 ex., 29.4–32.3 mm SL; 19°54'06" S 42°08'08" W, altitude about 660 m asl; A. M. Katz and P. J. Vilar do, 22 September 2022.

Diagnosis. *Trichomycterus caratinguensis* is distinguished from all other species of PAC by having a unique colour pattern combining LDPZ 1–3 represented by dark brown parallel stripes, with the LDPZ 2 and 3 stripes slightly converging on the caudal peduncle end (Figure 9; vs. never a similar colour pattern). *Trichomycterus caratinguensis* also differs from other congeners of PAC using the following combination of character states: 18–20 dorsal procurrent caudal-fin rays (vs. 22–28 in *T. altigrandensis*; *T. astromycterus*, *T. espinhacensis* Costa and Katz sp. nov., *T. macrophthalmus*, and *T. travassosi*); eight pectoral-fin rays (vs.

seven in *T. gasparinii* and *T. pantherinus*); S6 pore paired, pores separated by interspace (vs. single S6 median pore, sometimes two pores in close proximity in *T. alternatus*, *T. altipombensis*, *T. auroguttatus*, *T. astromycterus*, *T. brigadeirensis*, *T. castelensis*, *T. caudofasciatus*, *T. goeldii*, *T. jacupiranga*, *T. macrophthalmus*, *T. mimosensis*, and *T. travassosi*); presence of the anterior section of the infraorbital canal present (vs. absent in *T. gasparinii* and *T. pantherinus*); pointed mandibular teeth (vs. incisor-like in *T. astromycterus* and *T. jacupiranga*); 39–45 premaxillary teeth (vs. 25–34 in *Trichomycterus brigadeirensis* Costa, Katz and Vilardo sp. nov., *Trichomycterus caparaoensis* Costa, Barbosa and Katz sp. nov., *T. caudofasciatus*, and *T. travassosi*); a long nasal barbel, its tip reaching the opercle (vs. moderate in length or short, tip-reaching area nasal anterior to the opercle in *T. alternatus*, *T. altipombensis*, *T. castelensis*, *T. macrophthalmus*, *T. mimosensis*, *T. saquarema*, *T. travassosi*, and anterior to orbit in *T. astromycterus*); sesamoid supraorbital bone with a lateral expansion (vs. without lateral projections and processes in *T. caudofasciatus*, *T. puriventris*, *T. mimosensis*, *T. caparaoensis* Costa, Barbosa and Katz sp. nov., *T. castelensis* Costa, Katz and Vilardo sp. nov., and *T. vinnulus*), and 14 ribs (vs. 9–12 in *T. alternatus*, *T. altipombensis*, *T. astromycterus*, *T. auroguttatus*, *T. caudofasciatus*, *T. espinhacensis* Costa and Katz, sp. nov., *T. gasparinii*, *T. goeldii*, *T. jacupiranga*, *T. caudofasciatus*, *T. mimosensis*, *T. macrophthalmus*, *T. pantherinus*, *T. travassosi*, and *T. vinnulus*).

Table 2. Morphometric data of *Trichomycterus caratinguensis* Costa, Katz and Vilardo sp. nov.

	Holotype	Paratypes (n = 5)
Standard length (SL)	55.3	32.2–35.5
Percentage of standard length		
Body depth	13.1	12.7–14.9
Caudal peduncle depth	10.5	10.5–12.1
Body width	11.6	10.8–12.4
Caudal peduncle width	4.5	3.1–4.4
Pre-dorsal length	58.1	61.2–63.3
Pre-pelvic length	56.0	57.0–60.6
Dorsal-fin base length	10.3	11.5–13.5
Anal-fin base length	8.0	8.2–11.7
Caudal-fin length	14.7	15.5–19.9
Pectoral-fin length	14.6	14.5–16.3
Pelvic-fin length	10.9	10.8–13.4
Head length	19.3	21.6–23.4
Percentage of head length		
Head depth	91.0	80.2–97.0
Head width	162.4	147.7–173.2
Snout length	75.5	73.5–83.0
Interorbital width	53.9	46.5–55.1
Preorbital length	20.9	16.5–22.2
Eye diameter	23.1	23.5–32.3

Description. General morphology: Morphometric data are in Table 2. The dorsal surface of the head is nearly plain between orbits, with the eye not projected dorsally. Maxillary barbel posteriorly reaching area between an interopercular patch of odontodes and pectoral-fin base, rictal barbel reaching the middle portion of the interopercular patch of odontodes, nasal barbel reaching area just anterior to opercle. Jaw teeth pointed. Premaxillary teeth 39–45, slightly curved, arranged in irregular rows; dentary teeth 32–41, slightly curved backwards, irregularly arranged. Opercular odontodes 14–18, interopercular odontodes 34–40. Odontodes pointed, arranged in irregular rows. Anterior infraorbital canal present. s6 pore paired, nearer its symmetrical homologous pair than orbit. Dorsal and anal fins are subtriangular, margins slightly convex. Total dorsal-fin rays 11 or 12 (ii–iii + II + 7), total anal-fin rays 9 or 10 (ii–iii + II + 5). Anal-fin origin at vertical through dorsal-fin base posterior end. Pectoral-fin filament length is about 30% of pectoral-fin length without filament. Total pectoral-fin rays 8 (I + 7). Pelvic fin posteriorly reaching vertical through

middle of dorsal-fin base. Pelvic-fin bases are medially separated by interspace about equal pelvic-fin ray width. Total pelvic-fin rays 5 (I + 4). Caudal fin truncate. Total principal caudal-fin rays 13 (I + 11 + I), total dorsal procurrent rays 18–20 (xvii–xix + I), total ventral procurrent rays 13 or 14 (xii–xiii + I). Anus and urogenital papilla at vertical through anterior half of dorsal-fin base.

Osteology (Figures 3B, 5B and 6B): Anterior margin of mesethmoid concave, mesethmoid cornu rod-shaped. Lacrimal and sesamoid supraorbital narrow and flat, sesamoid supraorbital length about three times lacrimal length, with weak lateral expansion. The premaxilla is sub-rectangular in the dorsal view. Maxilla is boomerang-shaped, slender, slightly longer than premaxilla, with a small posterior process. Autopalatine sub-rectangular in dorsal view when excluding posterolateral process, its shortest width about half autopalatine length, lateral and medial margins slightly convex. The postero-lateral process of autopalatine is subtriangular; its length is about two-thirds of autopalatine length. Metapterygoid subtriangular, slightly deeper than long. Quadrate robust, dorsoposterior outgrowth in contact with hyomandibular outgrowth. Hyomandibula long, anterior outgrowth with a small concavity in its dorsal margin. The opercle is moderately elongated, the depth of the opercular odontode patch about four-fifths of the dorsal articular facet of the hyomandibula, and the dorsal process of the opercle is short and blunt. Interopercle long, about three-fourths of hyomandibula length. Preopercle compact, with small ventral expansion. Basibranchials 2 and 3 elongate without distinctive constrictions. Hypobranchial 1 is long, distal extremity slightly broader than the proximal extremity. Hypobranchials 2 and 3 are subtriangular and about equal in length. Parurohyal robust, lateral process relatively elongate, pointed, slightly curved; parurohyal head well-developed, with the prominent anterolateral paired process; middle foramen round, moderate; posterior process long, about four-fifths of the distance between anterior margin of parurohyal and anterior insertion of posterior process. Branchiostegal rays 7. Vertebrae 36 or 37. Ribs 14. Dorsal-fin origin at vertical through centrum of 16th or 17th vertebra; anal-fin origin at vertical through centrum of 21st or 22nd vertebra. One or two dorsal hypural plates, corresponding to hypurals 4 + 5 and 3, respectively; single ventral hypural plate corresponding to hypurals 1 and 2 and parhypural.

Colouration in alcohol (Figure 9): The ground colour of the flank and head is light yellowish grey. LDPZ 1–3 represented by dark brown parallel stripes. LDPZ-4 is represented by dispersed dark brown chromatophores. LDPZ 2, 3 and 4 slightly converge on the caudal peduncle end. Venter white. The dorsal surface of the head is dark brown, and the lateral surface is pale grey with a great concentration of dark brown spots. Nasal and maxillary barbels light brown, rictal barbel light grey. Fins hyaline, with small black spots on the basal portion of pectoral, dorsal and caudal fins. Specimens below 40 mm SL LDPZ 1–3 are represented by a longitudinal row of horizontally elongated black spots.

Colouration in life: Similar to colouration in alcohol, but with a concentration of yellow pigment on fin bases and head side.

Distribution and habitat. *Trichomycterus caratinguensis* is known only from streams draining a plateau about 650–700 m asl in the Rio Caratinga drainage, Rio Doce basin (Figure 8). The type locality is situated in a region where all the original vegetation cover has been lost, currently containing pastures, plantations and small urban centres, with rivers and streams showing strong signs of pollution. Where the species was found, Córrego Tabuleiro II is about 1.5–3.0 m wide, about 0.3 m deep, with a sandy bottom.

Etymology. The name *caratinguensis* is an allusion to this new species being presently only known from the Rio Caratinga drainage.

3.4. The *Trichomycterus goeldii* Complex

The *T. goeldii* complex, as delimited in Costa et al. [12], but also including a new species described below, is corroborated here. This clade has been diagnosed using three apomorphic features: 1—the presence of a long and robust postero-lateral process of the autopalatine (figure 2F in Ref. [10]; figure 2A,B in Ref. [12]); 2—a slightly folded maxilla (figure 2F in Ref. [10]; figure 2A,B in Ref. [12]); and 3—anterior cranial fontanel represented

using a minute aperture (figure 9B in Ref. [10]). Character states 1 and 2 are mostly observable in specimens above about 50 mm SL, in which the postero-lateral process of the autopalatine is broad and long, its length approximately equal or slightly longer than the autopalatine longitudinal length excluding the process and the anterior cartilage. Below this size, the anterior portion of the head is relatively shorter and bones of this region may have a different shape, including a slightly shorter and more slender postero-lateral process of the autopalatine and a less folded maxilla, making it difficult to evaluate the occurrence of character states 1 and 2 in species with only specimens below that size available for osteological examination. In addition, a long autopalatine postero-lateral process is also present in the more distantly related *T. vittulus* (Figure 5F), here considered as homoplastic conditions. The two apomorphic conditions are here confirmed to occur in all species examined of the *T. goeldii*. On the other hand, character state 3 is present in most specimens examined, but some variation precludes this condition as diagnostic for the clade.

This study corroborates two main lineages within the *T. goeldii* complex. The first lineage includes nominal species and populations with a conspicuous level of morphological divergence but low molecular differentiation. This geographically widespread clade (hereafter the W-clade) includes *T. auroguttatus* and *T. goeldii* from the Rio Paraíba do Sul basin and populations with indeterminate taxonomical status from the upper Rio Grande drainage, upper Rio Paraná basin, and Rio Muriaé and Rio Pomba drainages of the lower Rio Paraíba do Sul basin. This clade also includes an unnamed taxon (Figure 1) from the upper Rio Santo Antônio, RDB (Figure 8), represented in our collections by only four small specimens (UFRJ 13103, 2 ex.; UFRJ 13121, 2 ex. C&S). Due to the small available specimen sample, this taxon is not described here. It is identified as *Trichomycterus* sp. aff. *T. goeldii* and is supported as a sister to *T. auroguttatus* and *T. goeldii* (Figure 2).

The second lineage of the *T. goeldii* complex is endemic to the RDB (hereafter RDB1-clade) and is highly supported by molecular data (Figure 1), but no morphological apomorphy was found to be uniquely shared by species of this clade. The Doce-clade includes *T. alternatus* and *T. astromycterus*, two sympatric species supported as sister taxa, and *T. espinhacensis* Costa and Katz sp. nov. from the Rio Santo Antônio drainage, which is supported as sister to all other species of the Doce-clade. This clade also includes an unnamed species (figure 8 in Ref. [12]) previously identified as *T. alternatus* [12] from the lower Rio Piracicaba drainage (Figure 8). Additional material is still necessary to provide a formal description of this taxon, which is here identified as *Trichomycterus* sp. aff. *T. alternatus*, supported as sister to the clade comprising *T. alternatus* and *T. astromycterus* (Figure 2). Whereas *T. espinhacensis* Costa and Katz sp. nov. occurs in streams draining the Serra do Espinhaço, in altitudes between about 680–715 m asl, the other taxa of the RDB1-clade are found in lower altitude places, between about 280 and 350 m asl, close to the main course of the Rio Doce (Figure 8).

Trichomycterus espinhacensis Costa and Katz sp. nov.

LSID:urn:lsid:zoobank.org:act:1C174B5C-12E8-4BDF-AF24-8C7AF0EE668E

Figures 3C, 5C, 6C, 7C and 10; Table 3

Holotype. UFRJ 13483, 46.8 mm SL; Brazil: Minas Gerais State: Santo Antônio do Imbé Municipality: Rio Preto, tributary of Rio Guanhões, Rio Santo Antônio drainage, Rio Doce basin, 18°27'49" S 43°18'26" W, altitude about 715 m; W. J. E. M. Costa et al., 16 August 2022.

Paratypes. All from Brazil: Minas Gerais State: Rio Santo Antônio drainage, Rio Doce basin. Santo Antônio do Imbé Municipality: UFRJ 13118, 11 ex., 32.7–51.2 mm SL; UFRJ 13484, 3 ex. (C&S), 33.1–44.0 mm SL; UFRJ 13105, 3 ex. (DNA), 26.6–33.2 mm SL; collected with holotype. UFRJ 13123, 7 ex., 27.7–46.4 mm SL; CICC AA 07774, 3 ex., 40.1–40.4 mm SL; Rio Guanhões, 18°27'40" S 43°17'46" W, altitude about 700 m asl; W. J. E. M. Costa et al., 17 August 2022. Conceição do Mato Dentro Municipality: UFRJ 13478, 56.1 mm SL; UFRJ 13119, 17 ex., 34.9–47.6 mm SL; UFRJ 13120, 3 ex. (C&S), 42.8–47.0 mm SL; UFRJ 13108, 2 ex. (DNA), 40.5–48.3 mm SL; Córrego da Guinda, 19°00'54" S 43°35'07" W, altitude about 690 m; W. J. E. M. et al., 10 August 2022. UFRJ 13135, 2 ex., 24.8–30.9 mm SL; Cachoeira Três Barras, 19°05'58" S 43°29'13" W, altitude about 695 m; W. J. E. M. et al., 10 August 2022.



Figure 10. *Trichomycterus espinhacensis* Costa and Katz sp. nov. Holotype, UFRJ 13483, Santo Antônio do Imbé, 46.8 mm SL: (A) lateral, (B) dorsal, and (C) ventral views.

Table 3. Morphometric data of *Trichomycterus espinhacensis* Costa and Katz sp. nov.

	Holotype	Paratypes (n = 16)
Standard length (SL)	46.8	35.9–56.1
Percentage of standard length		
Body depth	17.1	15.5–21.2
Caudal peduncle depth	13.2	11.1–13.2
Body width	12.3	11.0–15.5
Caudal peduncle width	4.4	3.0–5.2
Pre-dorsal length	63.8	57.2–63.8
Pre-pelvic length	55.6	50.9–58.2
Dorsal-fin base length	11.7	10.2–13.7
Anal-fin base length	9.9	8.2–10.0
Caudal-fin length	18.0	16.0–19.6
Pectoral-fin length	14.9	13.3–17.7
Pelvic-fin length	12.0	11.3–14.1
Head length	20.8	19.9–23.0
Percentage of head length		
Head depth	47.4	42.9–59.3
Head width	83.1	78.4–91.3
Snout length	43.5	39.7–50.2
Interorbital width	23.4	20.4–29.5
Preorbital length	14.2	12.3–16.1
Eye diameter	16.5	15.1–21.5

Additional material (non-type specimens). UFRJ 13479, 49.8 mm SL; UFRJ 13122, 9 ex., 32.7–44.2 mm SL; UFRJ 13117, 3 ex. (C&S), 39.2–47.8 mm SL; UFRJ 13104, 5 ex. (DNA), 24.1–35.0 mm SL; Brazil: Minas Gerais State: Itambé do Mato Dentro: Rio Preto do Itambé, just below Cachoeira do Lúcio, Rio Santo Antônio drainage, Rio Doce basin, 19°24'50" S 43°19'49" W, altitude about 680 m; W. J. E. M. et al., 11 August 2022.

Diagnosis. *Trichomycterus espinhacensis* is distinguished from all other congeners of the *T. goeldii* complex, except *T. astromycterus*, by having 23–26 dorsal procurrent caudal-fin rays (vs. 17–19). *Trichomycterus espinhacensis* differs from *T. astromycterus* by having: a relatively long and thin mesethmoid cornu (Figure 5C; vs. short and robust, Figure 5G; see also figure 4 in Ref. [17], 2020); a relatively shorter maxilla, slightly longer than the premaxilla, without a distal widening (Figure 5C; vs. maxilla about one and half time longer than the premaxilla, with distinctive distal widening, Figure 5G; see also figure 3 in Ref. [17]); well-developed third hypobranchial ossification (Figure 7C; vs. rudimentary, Figure 7G); 35 or 36 vertebrae (vs. 33 or 34); the dorsal-fin origin at a vertical through the centrum of 17th vertebra (vs. 14th or 15th vertebra); a longer nasal barbel, its tip posteriorly reaching the opercle or the area just anterior to it (vs. reaching the area anterior to the orbit); and caudal fin subtruncate (vs. emarginate). *Trichomycterus espinhacensis* is also distinguished from all other species of the *T. goeldii* complex by having a rudimentary foramen on the parurohyal (Figure 6C; vs. well-developed) and a narrow, rod-shaped basibranchial 3 (vs. Figure 7C; vs. never rod-shaped, figure 3 in Ref. [12]). *Trichomycterus espinhacensis* also differs from *T. auroguttatus* and *T. goeldii* by having 36–39 premaxillary teeth (vs. 42–45), absence of a robust comma-shaped osseous core in the autopalatine articular shell for the lateral ethmoid (vs. presence; figure 2A,B in Ref. [12]), and a relatively narrow and long second hypobranchial (Figure 7C; vs. broad and short, figure 3A in Ref. [12]); and from *T. alternatus* by having a row of variably shaped small pale brown spots on LDPZ 3 (vs. row of black round spots, figure 2 in Ref. [6]).

Description. General morphology: Morphometric data are in Table 3. The dorsal surface of the head between orbits is plain to slightly concave, with the eye slightly projected dorsally. Maxillary barbel posteriorly reaching pectoral-fin base or area just anterior to it, rictal barbel reaching area between the middle and posterior part of an interopercular patch of odontodes, the tip of nasal barbel reaching opercle or area just anterior to it. Jaw teeth are pointed, slightly curved, irregularly arranged; premaxillary teeth 37–39; dentary teeth 29–33. Opercular odontodes 15–17, interopercular odontodes 30–33. Odontodes pointed, arranged in irregular rows Branchiostegal rays 7. s6 pore nearer to its symmetrical homologous s6 pore than to orbit. Dorsal and anal fins are subtriangular, anterior margin about straight, posterior margin slightly convex. Total dorsal-fin rays 11 or 12 (iii + II + 6–7), total anal-fin rays 10 (iii + II + 5). Anal-fin origin at vertical through the posterior part of dorsal-fin base, through the base of 5th or 6th branched dorsal-fin ray. Dorsal-fin origin at vertical through centrum of 17th vertebra; anal-fin origin at vertical through centrum of 21st vertebra. Pectoral-fin filament length is about 10–25% of pectoral-fin length without filament. Total pectoral-fin rays 8 (I + 7). Pelvic fin posteriorly reaching vertical at middle dorsal-fin base. Pelvic-fin bases are medially separated by small interspace. Total pelvic-fin rays 5 (I + 4). Caudal fin subtruncate, upper and lower corners rounded. Total principal caudal-fin rays 13 (I + 11 + I), total dorsal procurrent rays 24–26 (xxiii–xxv + I), total ventral procurrent rays 14 or 15 (xiii–xiv + I). Anus and urogenital papilla at vertical through dorsal-fin origin or immediately anterior to it.

Osteology (Figures 3C, 5C and 6C): Anterior margin of mesethmoid slightly concave, mesethmoid cornu rod-shaped. Lacrimal and sesamoid supraorbital narrow, rod-like, sesamoid supraorbital length about two times and half lacrimal length. The premaxilla is sub-rectangular in dorsal view, slightly tapering laterally. Maxilla boomerang-shaped, slender, longer than premaxilla, slightly folded in its main axis, with small projection on anteromedian margin and small posterior process. Autopalatine sub-rectangular in dorsal view when excluding posterolateral process, its shortest width about half autopalatine length, lateral margin about straight, medial margin sinuous, with deep concave. In the

postero-lateral process of autopalatine subtriangular, its length is about equal to autopalatine length without anterior cartilage. Metapterygoid subtrapezoidal, deeper than long. Quadrate robust, dorsoposterior outgrowth in close proximity with hyomandibular outgrowth. Hyomandibula long, anterior outgrowth with concave dorsal margin. The opercle is moderately elongated, the depth of the opercular odontode patch about three-fourths of the dorsal articular facet of the hyomandibula, and the dorsal process of the opercle is short and blunt. Interopercle long, about three-fourths of hyomandibula length. Preopercle compact, without ventral expansion. Basibranchials 2 and 3 elongate without distinctive middle constrictions; basibranchial 3 is rod-shaped. Hypobranchial 1 is long, distal extremity broader than proximal extremity. Hypobranchials 2 and 3 are subtriangular, about equal in length, and anterolaterally directed. Parurohyal robust, lateral process relatively elongate, pointed, slightly curved; parurohyal head well-developed, narrow, with prominent anterolateral paired process; middle foramen minute; posterior process moderate in length, about four-fifths distance between anterior margin of parurohyal and anterior insertion of posterior process. Vertebrae 35 or 36. Ribs 10 or 11. Two dorsal hypural plates, corresponding to hypurals 4 + 5 and 3, respectively; single ventral hypural plate corresponding to hypurals 1 and 2 and parhypural.

Colouration in alcohol (Figure 10): The ground colour of the dorsum, flank and head side is light brownish yellow on the dorsal part, gradually becoming lighter ventrally. Flank and dorsum with variably shaped small pale brown spots, their diameter approximately equal, slightly larger or slightly smaller than opercular patch of odontodes. LDPZ 1 spots sometimes longitudinally coalesced to form a stripe, sometimes transversely coalesced with LDPZ 2 spots. LDPZ 3 usually has round spots forming regular series, sometimes irregularly arranged and irregularly shaped. LDPZ 4 with paler spots. Dark chromatophores are scattered over the dorsal portion of the head and dorsal part of the trunk. Head with small light brown dots. Venter white. Nasal and maxillary barbels light brown, rictal barbel light grey. Fins hyaline, with dark brown chromatophores on the basal portion.

Colouration in life: Similar to colouration in alcohol.

Distribution and habitat. *Trichomycterus espinhacensis* is known from the upper course of tributaries of the Rio Santo Antônio drainage, middle Rio Doce basin, Serra do Espinhaço, in altitudes between about 680 and 715 m asl (Figure 8). This species was found to be associated with fine gravel bottom of clear water and fast-flowing streams. Specimens were collected above the bottom gravel.

Etymology. The name *espinhacensis* is an allusion to the occurrence of this new species in the Serra do Espinhaço, an important biodiversity centre of south-eastern Brazil.

3.5. The *Trichomycterus jacupiranga* Complex

The *T. jacupiranga* complex as delimited in Costa et al. [12], but also including a new species from the Serra do Caparaó below described, a new species from the Serra do Castelo below described, and *T. gasparinii*, not included in the previous analysis, was corroborated maximum support values. According to the phylogenetic analysis (Figure 2), the *T. jacupiranga* complex is sister to a clade containing the *T. puriventris* and *T. travassosi* complexes; the *T. jacupiranga* contains two subclades, one endemic to RDB (hereafter RDB2-clade), comprising *T. vinnulus*, a new species from the Serra do Caparaó, and a new species from the Serra do Castelo, and one endemic to smaller coastal basins (hereafter the C-clade), comprising *T. jacupiranga* and *T. gasparinii*.

The RDB2-clade is morphologically supported by the presence of a hypertrophied foramen of the parurohyal (Figure 6D–F), instead of being a smaller aperture as in other taxa of the *T. jacupiranga* complex and other congeners (Figure 6A–C), except species of a clade supported in Vilaro et al. [14] including *Trichomycterus melanopygius* Reis, Santos, Britto, Volpi and Pinna, 2020 and closely related species (see discussion below). Species of the RDB2-clade also share the presence of a peculiar morphology of the metapterygoid, in which the anterior region is slightly folded, resulting in an irregular quadrilateral shape (Figure 3D–F), thus contrasting with the subtriangular metapterygoid present in

other taxa of the *T. jacupiranga* complex and the great majority of congeners (Figure 3 in Ref. [10]). However, both character states relative to the metapterygoid (i.e., irregular quadrilateral and subtriangular shapes) occur in different lineages of *Psammocambeva*, making it difficult to establish character state polarization without ambiguities. Species of the RDB2-clade also differ from species of the C-clade by the absence of a distinctive lateral process in the sesamoid supraorbital (Figure 5D–F), which is present in both *T. gasparinii* and *T. jacupiranga*, and most other species congeners of PAC (Figure 5A–C,G). The phylogenetic analysis supported the new species from the Serra do Castelo as sister to a clade including *T. vinnulus* and the new species from the Serra do Caparaó (Figure 2), but no morphological apomorphic condition uniquely shared by these two last species was found.

Trichomycterus caparaoensis Costa, Barbosa and Katz sp. nov.

LSID:urn:lsid:zoobank.org:act:6CA6366D-631F-43DD-9AD6-99DA2D94F59A Figures 3D, 5D, 6D, 7D and 11; Table 4



Figure 11. *Trichomycterus caparaoensis* Costa, Barbosa and Katz sp. nov. Holotype, UFRJ 6006, Martins Soares, 53.4 mm SL: (A) lateral, (B) dorsal, and (C) ventral views.

Holotype. UFRJ 6006, 53.4 mm SL; Brazil: Minas Gerais State: Martins Soares Municipality: Córrego Feio, tributary of Rio José Pedro, Rio Manhuaçu drainage, Rio Doce basin, 20°23'37" S 41°51'31" W, altitude about 1015 m; W. J. E. M. Costa, B. B. Costa and C. P. Bove 24 December 2002.

Table 4. Morphometric data of *Trichomycterus caparaoensis* Costa, Barbosa and Katz sp. nov.

	Holotype	Paratypes (n = 11)
Standard length (SL)	53.4	34.7–47.6
Percentage of standard length		
Body depth	16.3	13.2–16.9
Caudal peduncle depth	11.7	10.7–12.0
Body width	12.5	9.3–12.0
Caudal peduncle width	3.8	2.4–4.3
Pre-dorsal length	63.9	60.8–65.9
Pre-pelvic length	60.0	55.7–60.2
Dorsal-fin base length	12.0	11.2–12.4
Anal-fin base length	9.8	8.1–9.9
Caudal-fin length	17.6	16.3–18.7
Pectoral-fin length	14.9	13.0–16.5
Pelvic-fin length	12.2	11.0–12.1
Head length	19.8	19.8–21.9
Percentage of head length		
Head depth	54.6	42.3–57.9
Head width	92.1	82.8–89.6
Snout length	45.9	38.2–45.3
Interorbital width	36.1	23.2–32.9
Preorbital length	13.7	9.6–13.6
Eye diameter	13.2	14.1–16.6

Paratypes. All from Brazil: Minas Gerais State: Rio Manhuaçu drainage, Rio Doce basin. Martins Soares Municipality: UFRJ 5676, 8 ex., 34.8–47.6 mm SL; UFRJ 7881, 2 ex., 42.8–47.0 mm SL; UFRJ 5682, 4 ex. (C&S), 40.5–48.3 mm SL; CICCAA 07775, 2 ex., 43.7–46.0 mm SL; collected with holotype. UFRJ 7044, 43.0 mm SL; Brazil: Minas Gerais State: Martins Soares Municipality: Poço das Crianças, Rio José Pedro, Rio Manhuaçu drainage, Rio Doce basin, 20°22'28" S 41°51'32" W, about 875 m asl; W. J. E. M. Costa, B. B. Costa and C. P. Bove, 24 December 2002. Iuna Municipality: UFRJ 13172, 2 ex. (DNA), 30.7–37.0 mm SL; Rio José Pedro, 20°22'09" S 41°51'28" W, about 800 m asl; A. M. Katz and P. Vilardo, 22 September 2022.

Diagnosis. *Trichomycterus caparaoensis* differs from all congeners of the *T. jacupiranga* complex by having the dorsal surface of the head between orbits slightly convex (vs. plain to slightly concave). *Trichomycterus caparaoensis* is distinguished from other species of the RDB2-clade by a colour pattern of LDPZ 3 in specimens above about 45 mm SL, consisting of a dark brown stripe interrupted in its posterior portion (vs. a row of dark brown to black spots). *Trichomycterus caparaoensis* is also distinguished from *T. vinnulus*, its hypothesised sister species, by having: a longer pectoral-fin filament (filament length about 30–50% of the pectoral fin, vs. about 10–20%); a relatively long interopercular patch of odontodes, longer than the largest horizontal length of the hyomandibular anterior outgrown (Figure 3D; vs. shorter, Figure 3F), more ribs (13 vs. 11); the postero-lateral process of the autopalatine postero-laterally directed, its length about two thirds of the autopalatine length (Figure 5D; vs. posteriorly directed, its length about equal autopalatine length, Figure 5F); the second hypobranchial short, about so long as the third hypobranchial (Figure 7D; vs. long, about twice longer than the third hypobranchial, Figure 7F); and the posterior process of the parurohyal short, about half the distance between the anterior margin of the parurohyal and the anterior insertion of the posterior process (Figure 6D; vs. about equal or slightly shorter, Figure 6F). *Trichomycterus caparaoensis* is also distinguished from *T. castelensis* and *T. jacupiranga* by having paired S6 pore (vs. a single S6 median pore) and fewer opercular odontodes (11–15 vs. 17–19); from *T. gasparinii* by the presence of the anterior section of the infraorbital canal (vs. absence) and eight pectoral-fin rays (vs. seven); and from *T. jacupiranga* by having pointed mandibular teeth (vs. incisor-like).

Description. General morphology: Morphometric data are in Table 4. The dorsal surface of the head between orbits is slightly convex, with the eye not projected dorsally. Maxillary barbel posteriorly reaching pectoral-fin base, rictal barbel reaching posterior part of an interopercular patch of odontodes, the tip of nasal barbel reaching opercle. Jaw teeth pointed. Premaxillary teeth 25–35, slightly curved, arranged in irregular rows; dentary teeth 30–41, slightly curved backwards, irregularly arranged. Opercular odontodes 9–13, interopercular odontodes 31–42. Odontodes pointed, arranged in irregular rows. Anterior infraorbital canal present. s_6 pore nearer to its symmetrical homologous s_6 pore than to orbit. Dorsal and anal fins are subtriangular, anterior margin about straight, posterior margin slightly convex. Total dorsal-fin rays 12 (iii + II + 7), total anal-fin rays 10 (iii + II + 5); anal-fin origin at vertical through the posterior part of dorsal-fin base. Pectoral-fin filament length is about 30–50% of pectoral-fin length without filament. Total pectoral-fin rays 8 (I + 7). Pelvic fin posteriorly reaching vertical just posterior to middle dorsal-fin base. Pelvic-fin bases are medially separated by a small interspace, about half-length pelvic-fin base. Total pelvic-fin rays 5 (I + 4). Caudal fin subtruncate, upper and lower corners rounded. Total principal caudal-fin rays 13 (I + 11 + I), total dorsal procurrent rays 16–18 (xv–xvii + I), total ventral procurrent rays 13 or 14 (xii–xiii + I). Anus and urogenital papilla at vertical through anterior portion of dorsal-fin base.

Osteology (Figures 3D, 5D, 6D and 7D): Anterior margin of mesethmoid nearly straight, mesethmoid cornu subtriangular in dorsal view. Lacrimal and sesamoid supraorbital narrow, rod-like, sesamoid supraorbital length about two times lacrimal length. The premaxilla is sub-rectangular in dorsal view, slightly tapering laterally. Maxilla is boomerang-shaped, slender, slightly longer than premaxilla, with a minute posterior process. Autopalatine sub-rectangular in dorsal view when excluding posterolateral process, its shortest width about half autopalatine length, lateral margin about straight, medial margin slightly concave. The postero-lateral process of autopalatine is subtriangular; its length is about two-thirds of autopalatine length. Metapterygoid subtrapezoidal, slightly longer than deep. Quadrate robust, dorsoposterior outgrowth in contact with hyomandibular outgrowth. Hyomandibula long, anterior outgrow shallow, with a steep concavity in the middle portion of dorsal margin. The opercle is moderately elongated; the depth of the opercular odontode patch is about two-thirds of the dorsal articular facet of the hyomandibula; the dorsal process of the opercle is short and blunt. Opercular odontodes 13–15, odontodes pointed, arranged in irregular transverse rows. Interopercle long, about three-fourths of hyomandibula length. Interopercular odontodes 31–42, odontodes pointed, arranged in irregular longitudinal rows. Preopercle compact, without ventral expansion. Basibranchials 2 and 3 elongate without distinctive constrictions. Hypobranchial 1 long, distal extremity slightly broader than proximal extremity. Hypobranchials 2 and 3 are subtriangular and about equal in length. Parurohyal robust, lateral process relatively elongate, pointed, slightly curved; parurohyal head well-developed, with prominent anterolateral paired process; middle foramen oval; posterior process short, about half distance between anterior margin of parurohyal and anterior insertion of posterior process. Branchiostegal rays 7. Vertebrae 36 or 37. Ribs 13. Dorsal-fin origin at vertical through centrum of 19th or 20th vertebra; anal-fin origin at vertical through centrum of 23rd or 24th vertebra. Two dorsal hypural plates, corresponding to hypurals 4 + 5 and 3, respectively; single ventral hypural plate corresponding to hypurals 1 and 2 and parhypural.

Colouration in alcohol (Figure 11): The ground colour of the dorsum, dorsal portion of flank and head side is pale brownish yellow, becoming lighter on the ventral part of flank and head side. LDPZ 1 and 2 are represented by pale brown round spots longitudinally in close proximity, sometimes coalesced. LDPZ 3 is represented by a dark brown stripe interrupted in its posterior portion. In some specimens below about 45 mm SL and all specimens below about 35 mm SL, LDPZ 3 is represented by separate dark brown blotches. LDPZ 4 is represented by dark brown melanophores more concentrated on the posterior half of the flank, forming small rounded marks with diffuse limits. Venter white. Odontode patches are light grey. Barbels are light grey. Unpaired fins are hyaline, with dark brown

chromatophores concentrated on rays and a vertical series of brown spots on the caudal-fin base, sometimes forming diffuse bars. Paired fins are hyaline, with brown dots on the pectoral-fin base.

Colouration in life: Similar to colouration in alcohol, but with pale golden dots above LDPZ 3.

Distribution and habitat. *Trichomycterus caparaoensis* is known only from the upper Rio Manhuaçu tributaries draining the Serra do Caparaó (Figure 8). The species was found in clear water, fast-flowing streams with forested margins, and with gravel, sand and rocks on the bottom, in altitudes between about 800 and 1015 m asl. Specimens were collected above the bottom gravel.

Etymology. The name *caparaoensis* is an allusion to this new species presently being known only from the Serra do Caparaó region.

Trichomycterus castelensis Costa, Katz and Vilar do sp. nov.

LSID:urn:lsid:zoobank.org:act:3CCC62D6-67EC-4C10-8388-442551EDBAE4

Figures 3E, 5E, 6E, 7E and 12; Table 5

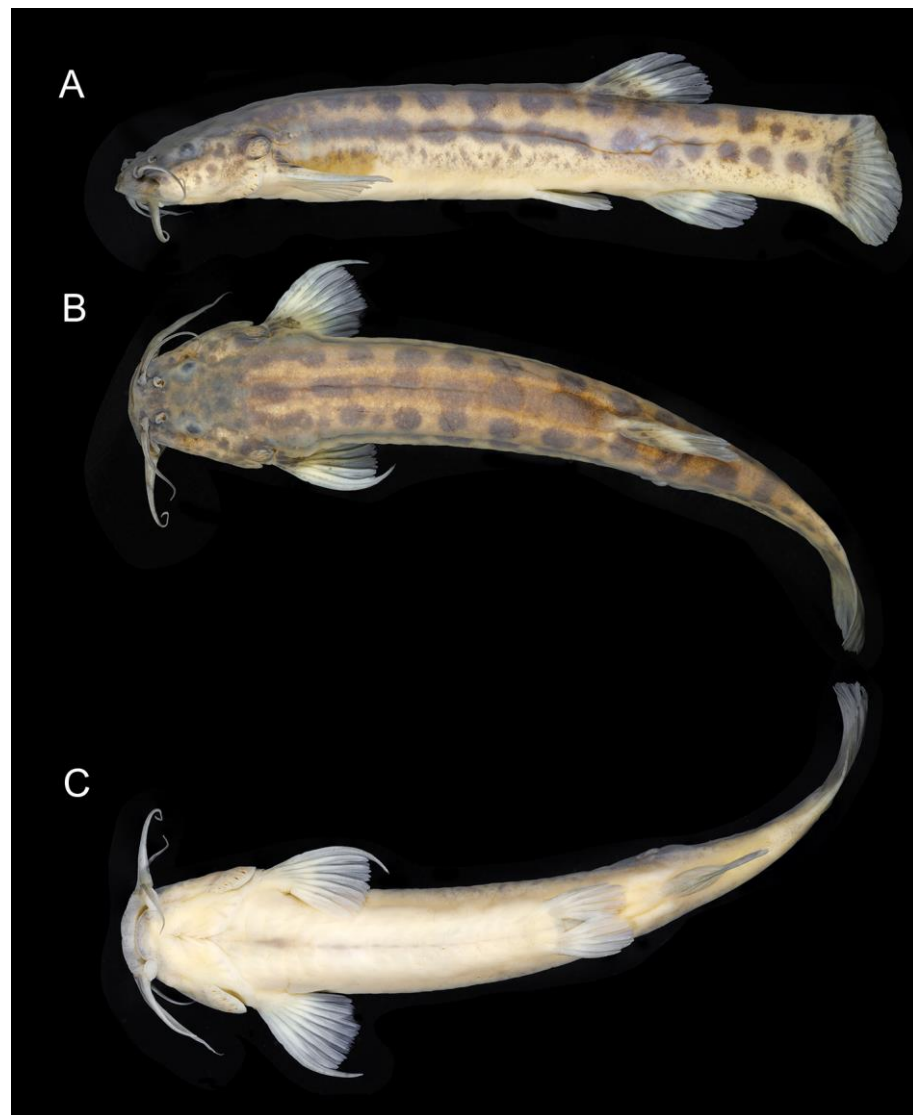


Figure 12. *Trichomycterus castelensis* Costa, Katz, and Vilar do sp. nov. Holotype, UFRJ 13481, Afondo Claudio, 63.3 mm SL: (A) lateral, (B) dorsal, and (C) ventral views.

Table 5. Morphometric data of *Trichomycterus castelensis* Costa, Katz, and Vilardo, sp. nov.

	Holotype	Paratypes (n = 10)
Standard length (SL)	63.3	37.9–57.1
Percentage of standard length		
Body depth	15.1	13.3–15.2
Caudal peduncle depth	11.7	11.1–12.3
Body width	13.1	10.5–12.5
Caudal peduncle width	4.3	3.4–4.3
Pre-dorsal length	63.7	61.4–65.5
Pre-pelvic length	58.1	56.1–59.7
Dorsal-fin base length	11.0	11.0–14.0
Anal-fin base length	9.9	8.2–11.3
Caudal-fin length	16.2	15.5–21.8
Pectoral-fin length	14.6	13.1–16.5
Pelvic-fin length	11.3	11.3–13.5
Head length	20.7	20.7–23.1
Percentage of head length		
Head depth	49.0	46.6–51.1
Head width	87.9	83.4–91.9
Snout length	46.7	10.9–43.8
Interorbital width	30.6	25.6–28.6
Preorbital length	15.0	10.3–13.5
Eye diameter	14.2	12.5–18.0

Holotype. UFRJ 13481, 63.3 mm SL; Brazil: Minas Gerais State: Afonso Claudio Municipality: small stream tributary to Rio Boa Sorte, Rio Guandu drainage, Rio Doce basin, 20°11'40" S 41°03'42" W, altitude about 630 m, Serra do Castelo; A. M. Katz and P. Vilardo, 20 September 2022.

Paratypes. UFRJ 13250, 17 ex., 21.9–57.1 mm SL; UFRJ 13482, 4 ex. (C&S), 33.6–51.1 mm SL; UFRJ 13251, 3 ex., 20.2–40.0 mm SL; UFRJ 13108, 1 ex. (DNA), 40.2 mm SL; CICC AA 07776, 3 ex., 40.6–49.3 mm SL; collected with holotype.

Diagnosis. *Trichomycterus castelensis* is distinguished from all other congeners of the *T. jacupiranga* complex by the following combination of character states: LDPZ-3 being represented by a row of dark brown to black spots, decreasing in size posteriorly, their diameter usually greater or sometimes nearly equal to opercular odontode diameter, anterior-most spots sometimes longitudinally coalesced (vs. a dark brown stripe interrupted in its posterior portion in *T. caparaoensis*); the dorsal surface of head between orbits slightly concave (vs. convex in *T. caparaoensis*); a relatively long interopercular patch of odontodes, longer than the largest horizontal length of the hyomandibular anterior outgrown (Figure 3E; vs. shorter in *T. vinnulus*, Figure 3F); 14 ribs (vs. 10 or 11 in *T. gasparinii*, *T. jacupiranga*, and *T. vinnulus*); the postero-lateral process of the autopalatine postero-laterally directed, its length about two thirds or less of the autopalatine length (Figure 5E; vs. posteriorly directed, its length about equal autopalatine length in *T. vinnulus*, Figure 5F); the second hypobranchial short, about so long as the third hypobranchial (Figure 7E; vs. long, about twice longer than the third hypobranchial in *T. vinnulus*, Figure 7F); the posterior process of the parurohyal long, about eight tenths of the distance between the anterior margin of the parurohyal and the anterior insertion of the posterior process (Figure 6E; vs. short, about half the distance in *T. castelensis*, Figure 6F); a single S6 median pore (vs. paired S6 pore in *T. caparaoensis* and *T. gasparinii*); opercular odontodes 17–19 (vs. 11–15 in *T. caparaoensis*); anterior section of the infraorbital canal present (vs. absent in *T. gasparinii*); eight pectoral-fin rays (vs. seven in *T. gasparinii*); and pointed mandibular teeth (vs. incisor-like in *T. jacupiranga*). *Trichomycterus castelensis* is also distinguished from all other congeners of PAC by having a relatively shorter autopalatine postero-lateral process (Figure 5E), its length about two-fifths of autopalatine length (vs. three-fifths or more).

Description. General morphology: Morphometric data are in Table 5. The dorsal surface of the head between orbits is slightly concave, and the eye is slightly projected dorsally. Maxillary barbel posteriorly reaching pectoral-fin base, rictal barbel reaching a middle portion of an interopercular patch of odontodes, nasal barbel reaching the area just anterior to opercle. Jaw teeth pointed. Premaxillary teeth 39–42, slightly curved, arranged in irregular rows; dentary teeth 40–50, slightly curved backwards, irregularly arranged. Opercular odontodes 17–19, interopercular odontodes 36–40. Odontodes pointed, arranged in irregular rows. Anterior infraorbital canal present. Single median s6. Dorsal and anal fins are subtriangular, margins slightly convex. Total dorsal-fin rays 12 (iii + II + 7), total anal-fin rays 10 (iii + II + 5). Anal-fin origin at vertical through dorsal-fin base posterior end or just posterior to it. Pectoral-fin filament length is about 20–40% of pectoral-fin length without filament. Total pectoral-fin rays 8 (I + 7). Pelvic fin posteriorly reaching vertical just posterior to middle dorsal-fin base. Pelvic-fin bases are medially separated by interspace about three-fourths pelvic-fin base. Total pelvic-fin rays 5 (I + 4). Caudal fin subtruncate, upper and lower corners rounded. Total principal caudal-fin rays 13 (I + 11 + I), total dorsal procurent rays 17–21 (xvi–xix + I), total ventral procurent rays 13–15 (xii–xiv + I). Anus and urogenital papilla at vertical through area just anterior to middle of dorsal-fin base.

Osteology (Figures 3E, 5E, 6E and 7E): Anterior margin of mesethmoid slightly concave, mesethmoid cornu rod-shaped. Lacrimal and sesamoid supraorbital narrow and flat, sesamoid supraorbital length about three times lacrimal length. The premaxilla is sub-rectangular in the dorsal view. Maxilla is boomerang-shaped, slender, slightly longer than premaxilla, with a minute posterior process. Autopalatine is sub-rectangular in the dorsal view when excluding the posterolateral process; its shortest width is about two-fifths autopalatine length, lateral margin slightly convex, and medial margin with pronounced concavity. The postero-lateral process of autopalatine is subtriangular and short, its length about two-fifths of autopalatine length. Metapterygoid subtrapezoidal, slightly deeper than long. Quadrate robust, dorsoposterior outgrowth in contact with hyomandibular outgrowth. Hyomandibula long, anterior outgrowth shallow. The opercle is moderately elongated; the depth of the opercular odontode patch is about two-thirds of the dorsal articular facet of the hyomandibula, and the dorsal process of the opercle is short and blunt. Interopercle long, about three-fourths of hyomandibula length. Preopercle compact, without ventral expansion. Basibranchials 2 and 3 elongate, slightly constricted at the middle portion. Hypobranchial 1 long, distal extremity slightly broader than proximal extremity. Hypobranchials 2 and 3 are subtriangular and about equal in length. Parurohyal robust, lateral process relatively elongate, pointed, slightly curved; parurohyal head well-developed, with the prominent anterolateral paired process; middle foramen round, large; posterior process long, about eight-tenths of distance between anterior margin of parurohyal and anterior insertion of posterior process. Branchiostegal rays 6 or 7. Vertebrae 37. Ribs 14. Dorsal-fin origin at vertical through centrum of 20th vertebra; anal-fin origin at vertical through centrum of 24th vertebra. Two dorsal hypural plates, corresponding to hypurals 4 + 5 and 3, respectively; single ventral hypural plate corresponding to hypurals 1 and 2 and parhypural.

Colouration in alcohol (Figure 12): The ground colour of the flank and dorsum is light brownish yellow, gradually becoming lighter ventrally, and the colour ground of the dorsum is light brown. LDPZ 1–4 comprising dark brown to black round spots. LDPZ 1 spots sometimes coalesced with neighbouring LDPZ 2 and 3 spots to form transverse bars. LDPZ 3 spots decreasing in size posteriorly, anterior-most spots sometimes longitudinally coalesced. LDPZ 4 is represented by dispersed dark brown chromatophores, not forming distinctive marks. Venter white. The dorsal surface of the head is brown, and the lateral surface is light brownish yellow with irregularly diffuse dark brown chromatophores, more concentrated above the opercle. Nasal barbel light brown, maxillary and rictal barbels light grey. Fins hyaline, with small black spots on the basal portion of the pectoral and unpaired fins. Adults and juveniles with similar colour patterns.

Colouration in life: Similar to colouration in alcohol, with minute patches of golden iridescence on the dorsum and dorsal part of the flank.

Distribution and habitat. *Trichomycterus castelensis* is known only from the type locality area, in a stream tributary to the Rio Boa Sorte, Rio Guandu drainage at the Serra do Castelo, about 630 m asl, Rio Doce basin (Figure 8). The site where the species was collected is clear water and fast-flowing streams, about 1 m wide and 0.3 wide, with gravel, sand and rocks on the bottom and secondary vegetation on the banks. Specimens were collected below rocks.

Etymology. The name *castelensis* refers to the occurrence of the new species in the Serra do Castelo region.

4. Discussion

4.1. Phylogenetic Relationships and Distribution Patterns in RDB

Costa et al. [12] identified four main lineages within PAC and then named species complexes. However, support values for these lineages and for relationships among them were low in most tree nodes. The present analysis involving larger genetic and taxon samples yielded a more robust phylogeny, with high support values in most tree nodes (Figure 2). Among the main PAC lineages, three occur in RDB: the first one comprising *T. brigadeirensis* alone, which is sister to a well-supported clade including all other species of PAC; the second including *T. caratinguensis* alone, weakly supported as sister to *T. goeldii* complex (see results above); the third comprising the *T. goeldii* complex; and the fourth comprising the *T. jacupiranga* complex (Figure 2). The distribution of these lineages in RDB is nearly disjunct (Figure 8), with *T. brigadeirensis* occurring in the southern-most portion of the basin, the *T. goeldii* complex occurring in the western one, *T. caratinguensis* in the central one, and the *T. jacupiranga* complex in the southern portion. The areas occupied by the *T. goeldii* and *T. jacupiranga* complexes overlap in the area comprising the upper-middle course of the main channel of the Rio Doce, the only place in the basin where different species of PAC area are found in sympatry.

4.2. Areas of Endemism for *Trichomycterines* in RDB

Delimitation of areas of endemism is crucial for the implementation of conservation strategies in large and complex river basins, combining high species diversity and accentuated levels of environmental disturbance [13]. Distribution patterns of PAC species in RDB corroborate five areas of endemism for trichomycterines that are shared by other congeners: A—Serra do Espinhaço, B—Serra do Brigadeiro, C—Serra do Caparaó, D—Serra do Castelo, and E—the upper-middle main course of the Rio Doce (Figure 8). The first four correspond to mountain ranges ('serras' in Portuguese), and the first three are known to be important biodiversity centres with high rates of plant and animal endemism.

The Serra do Espinhaço is among the most important centres of plant diversity in the world, with high rates of endemism [1]. With peaks reaching about 2000 m asl, the southern plateau of the Serra do Espinhaço is situated in a transition area between the Cerrado savanna and the Atlantic Forest, being a main divider between the Rio Doce, Rio Jequitinhonha, and Rio São Francisco basins. Presently, two species of *Trichomycterus* are known to be endemic to rivers of RDB draining the eastern slope of the southern plateau of the Serra do Espinhaço: *T. espinhacensis* here described and *Trichomycterus brucutu* Reis and de Pinna, 2022. *Trichomycterus illuvies* Reis and de Pinna, 2022 was also described for this region, but according to Reis and de Pinna [6], it also occurs in the distant Ribeirão Sacramento, draining the northern Serra da Mantiqueira region. This area of endemism is congruent with results for the unity of analysis (UA) Santo Antônio delimited by Sarmento-Soares et al. [37] analysing endemism of the ichthyofauna in RDB. The area of the Serra do Espinhaço drained by the Rio Doce includes some small State Park reserves, but most of this drainage area is unprotected and intensively exploited by mining enterprises.

The Serra do Brigadeiro is a separate nucleus of the northern plateau of the Serra da Mantiqueira, with the highest peak reaching 1985 m in altitude, sheltering headwaters

belonging to the Rio Doce basin and the Rio Paraíba do Sul basin. The Serra do Brigadeiro region has been identified as an important centre of plant and animal biodiversity, with new species continually being described, with frogs standing out among vertebrates [38]. At present, two trichomycterine species are known from Serra do Brigadeiro, both endemic to the upper Rio Casca drainage, Rio Doce basin ([39]; this study), *T. brigadeirensis* here described and *Trichomycterus argos* Lezama, Triques and Santos, 2012, a member of the subgenus *Cryptocambeva* [12]. Although no sample was made in the Serra do Brigadeiro State Park, its proximity to our collecting sites indicates a potential role in protecting endemic trichomycterine species.

The Serra do Caparaó represents the main nucleus of the northern plateau of the Serra da Mantiqueira, with the highest peak, Pico da Bandeira, reaching 2891 m asl, being a natural divider among the Rio Itabapoana, Rio Itapemirim, Rio Doce, and Rio Paraíba do Sul basins. It is among the most important centres of biodiversity of the Atlantic Forest for plants [40], also sheltering a great diversity of animals (e.g., [41]), including an endemic genus of microteiid lizard [42]. Two species of *Trichomycterus* were formerly described from the southern slope of the Serra do Caparaó, *T. caudofasciatus* and *Trichomycterus brunoi* Barbosa and Costa, 2010 [43,44], whereas two species have been recorded in the northern slope of the Serra do Caparaó drained by the RDB, *T. caparaoensis* here described, and *T. brunoi* of the subgenus *Cryptocambeva*, recently recorded for this basin [6]. This area is also corroborated by the distribution patterns in the UA Manhuaçu [37]. Most of this area is protected by the Caparaó National Park. However, no collection was made inside the limits of this park. In the area outside of the park boundaries where several individuals of *T. caparaoensis* were collected in 2002, no specimens were found in 2022, suggesting a potentially alarming decline.

The Serra do Castelo is a smaller mountain range sheltering headwaters of rivers of the lower RDB and smaller coastal basins, with the highest peaks reaching about 2000 m asl. Presently, two trichomycterines are known to be endemic to the rivers of RDB draining the Serra do Castelo area, *T. castelensis* here described, and *Trichomycterus barrocos* Reis and de Pinna, 2022 [6]. This area is partially corroborated by the distribution patterns in UA Santa Maria do Rio Doce/Guandu described by Sarmiento et al. [37].

Finally, the upper-middle main course of the Rio Doce corresponds to an area drained by the Rio Doce and neighbouring tributaries in altitudes about 280–350 m asl. This is the only place where three different species of PAC, *T. alternatus*, *T. astromycterus*, and *T. vinnulus* may be found in sympatry. *Trichomycterus tantalus* Reis and de Pinna, 2022 also exhibit a similar distribution pattern [6], thus corroborating the upper-middle main course of the Rio Doce as an area of endemism for trichomycterine catfishes.

4.3. Comparing Species Diversity of Trichomycterines in RDB and in the Rio Paraíba do Sul Basin

Studies on trichomycterines from RDB were rare until recently, with a single endemic species recorded for the basin before the present century [16,17]. This historical record contrasts with the several records of trichomycterines for the Rio Paraíba do Sul basin since the 19th and 20th centuries [10,16,17,45–47], with an area only about 65% of RDB. Breaking the long period of omission about trichomycterines from the RDB, Lezama et al. [39] described *T. argos*, of the subgenus *Cryptocambeva*, and Reis and collaborators described nine species [6,18,48], all of the subgenus *Psammocambeva* [14].

Recent studies indicated the existence of at least 21 trichomycterine species endemic to the Rio Paraíba do Sul basin ([12,49,50] and included references), belonging to five different subgenera (i.e., *Cryptocambeva*, *Humboldtglanis*, *Paracambeva*, *Psammocambeva*, and *Trichomycterus*; [10]). Contrastingly, today, there are 16 nominal species of *Trichomycterus* considered endemic to RDB, of which 15 belong to *Psammocambeva* and only one, *T. argos*, belongs to *Cryptocambeva*. A recent biogeographic analysis indicated that the occurrence of *T. argos* and *T. brunoi*, of the subgenus *Cryptocambeva*, in the Rio Doce and Rio Itabapoana basins is derived from a recent dispersal event in this region [14]. These data suggest that the Rio Paraíba do Sul basin contains vestiges of older radiation of *Trichomycterus s.s.*,

since presently it is home to species descending from all the main intrageneric lineages, which had their origin during the Oligocene, about 23.9 Ma according to Vilardo et al. [14], whereas species diversification in RDB took place much later, probably after the initial diversification of *Psammocambeva* during the Miocene, about 14.6 Ma or later [14].

5. Conclusions

The RDB is situated in a tropical region with a rich diversity of mountain and lowland habitats, encompassing a considerable portion of the Atlantic Forest, considered one of the most important and most endangered biodiversity hotspots in the world [51]. Recent studies have revealed a great diversity of undescribed small fish species that are endemic to this basin (see introduction above), although large areas of the basin are intense and continuously disturbed by anthropic activities. Following Costa et al. [13], this study reinforces the importance of accelerating the pace of naming new taxa and delimitating areas of greater concentration of endemic species as a primary tool for conservation-based strategies.

Author Contributions: Conceptualization, W.J.E.M.C.; data obtaining, W.J.E.M.C., J.L.O.M., M.A.B., P.J.V. and A.M.K.; formal analysis, W.J.E.M.C. and J.L.O.M.; investigation and data curation, W.J.E.M.C., J.L.O.M., M.A.B., P.J.V. and A.M.K.; writing—original draft preparation, W.J.E.M.C.; writing—final version, W.J.E.M.C., J.L.O.M. and A.M.K.; visualization, W.J.E.M.C., J.L.O.M. and A.M.K.; supervision, W.J.E.M.C.; project administration, W.J.E.M.C.; funding acquisition, W.J.E.M.C., P.J.V. and A.M.K. All authors have read and agreed to the published version of the manuscript.

Funding: This study was funded by Conselho Nacional de Desenvolvimento Científico e Tecnológico (CNPq; grant 304755/2020-6 to WJEMC and 140689/2022-2 to PJV), Fundação Carlos Chagas Filho de Amparo à Pesquisa do Estado do Rio de Janeiro (FAPERJ; grant E-26/201.213/2021 to WJEMC, E-26/202.327/2018 to JLOM; and E-26/202.005/2020 to AMK). This study was also supported by CAPES (Finance Code 001) through the Programa de Pós-Graduação em: Biodiversidade e Biologia Evolutiva/UFRJ and Genética/UFRJ.

Institutional Review Board Statement: The animal study protocol was approved by the Ethics Committee for Animal Use of the Federal University of Rio de Janeiro (protocol code: 065/18, approved in August 2018).

Informed Consent Statement: Not applicable.

Data Availability Statement: DNA sequences used in this study are deposited in GenBank.

Acknowledgments: We are grateful to C. P. Bove and B. B. Costa for help during field collections; M. Petrungraro, L. I. Chaves, L. Santos, and L. Neves for technical assistance; and the technical staff of the Fish collection of the Field Museum of Natural History (Zoology), including K. A. Swagel and M. W. Littmann that authored images at the museum site, for making available photos and radiographs of type specimens. The manuscript benefited from the criticisms made by three anonymous reviewers.

Conflicts of Interest: The authors declare no conflict of interest. The funders had no role in the design of the study; in the collection, analyses, or interpretation of data; in the writing of the manuscript; or in the decision to publish the results.

Appendix A

Terminal taxa for molecular phylogeny and respective GenBank accession numbers.

	Mitochondrial Genes			Nuclear Genes	
	COX1	CYTB	ND4	MYH6	RAG2
<i>Nematogenys inermis</i>	KY857952	—	AY307250.1	KY858107	KY858182
<i>Trichogenes longipinnis</i>	MK123682	MK123704	MN389484.1	MF431104	MF431117
<i>Microcambeva ribeirae</i>	MN385807	OK334290	MN389502.1	MN385819	MN385832
<i>Ituglanis boitata</i>	MK123684	MK123706	MN389485.1	MF431105	MK123758
<i>Scleronema minutum</i>	MK123685	MK123707	MN389486.1	MK123735.1	MK123759.1
<i>Cambeva barbosa</i>	MK123689	MK123713	MN389487.1	MK123740.1	MN385820

	Mitochondrial Genes			Nuclear Genes	
	COX1	CYTB	ND4	MYH6	RAG2
<i>Trichomycterus itatiayae</i>	MW671552	MW679291	—	OL779229	OL779233
<i>Trichomycterus nigricans</i>	MN813005	MK123723	MN389488.1	MK123750	MK123765
<i>Trichomycterus albinotatus</i>	MN813007	MK123716	OM324337.1	MK123743	MN812990
<i>Trichomycterus brasiliensis</i>	MK123691	MK123717	OM324347.1	MK123744	MK123763
<i>Trichomycterus travassosi</i>	MK123701	MK123730	OR356037	MK123756	OL752425
<i>Trichomycterus</i> sp. aff. <i>T. alternatus</i>	MK123690	MK123715.1	OR356038	MK123742.1	MN812991.1
<i>Trichomycterus pantherinus</i>	MK123697.1	MK123725	OR356039	MK123752	MN812989
<i>Trichomycterus goeldii</i>	MT435136	MT436453	OR356040	MT436451	MT446427
<i>Trichomycterus jacupiranga</i>	OL764372	OL779234	OR356041	OL779230	OL779232
<i>Trichomycterus pradensis</i>	MN813003.1	MK123726.1	OR356042	MK123753.1	MN812988.1
<i>Trichomycterus melanopygius</i>	OQ357896	OQ355720	—	OQ355731	OQ400967
<i>Trichomycterus auroguttatus</i>	MT435135	MT436452.1	OR356043	MT436450	OP699434.1
<i>Trichomycterus saquarema</i>	OP698258	OP688464.1	OR356044	—	OP688470
<i>Trichomycterus macrophthalmus</i>	OL741727	OL752426	OR356045	OL752418	OL752421
<i>Trichomycterus astromycterus</i>	ON036881	OK652453	OR356046	OK652451.1	OK652448.1
<i>Trichomycterus altipombensis</i>	OP698260	OP688466.1	—	—	OP688472
<i>Trichomycterus purioventris</i>	OP698259	OP688465.1	OR356047	OP688468	OP688471
<i>Trichomycterus mimosensis</i>	OQ357893	OQ355719	13139	—	OQ400966
<i>Trichomycterus longibarbatus</i>	OQ357895	OQ355718	OR356048	—	OQ400965
<i>Trichomycterus castelensis</i>	OR354435	OR356030	OR356049	—	OR356058
<i>Trichomycterus caparaoensis</i>	OR354436	OR356031	OR356050	—	OR356059
<i>Trichomycterus gasparinii</i>	OR354437	OR356032	OR356051	—	OQ400962
<i>Trichomycterus vinnulus</i>	ON036819.1	OK652452	OR356052	OK652450	OK652449
<i>Trichomycterus brigadeirensis</i>	OR354438	OR356033	OR356053	—	OR356060
<i>Trichomycterus caratinguensis</i>	OR354439	OR356034	OR356054	—	OR356061
<i>Trichomycterus</i> sp. aff. <i>T. goeldii</i>	OR354440	OR356035	OR356055	—	OR356062
<i>Trichomycterus espinhacensis</i>	OR354441	OR356036	OR356056	—	OR356063
<i>Trichomycterus alternatus</i>	OQ357886	OQ355710	OQ355721	MK123742	OQ400957
<i>Trichomycterus caudofasciatus</i>	—	MK123719	OR356057	MK123719	MK123764

Appendix B

Best-fitting partition schemes and evolutive models. The following evolutionary models were used: Tamura-Nei (TRN) [52], Hasegawa-Kishino-Yano (HKY) [53], General Time Reversible (GTR) [54], Symmetrical model (SYM) [55], Kimura 2-parameter (K80) [56].

Partition	Base Pairs	Evolutive Model
COX1 1st	174	TRN+G
COX1 2nd	174	HKY+I
COX1 3rd	173	GTR+G
CYTB 1st	363	SYM+I+G
CYTB 2nd	363	TRN+I
CYTB 3rd	362	GTR+I+G
ND4 1st	231	TRN+G
ND4 2nd	230	TRN+G
ND4 3rd	231	HKY+G
RAG2 1st + MYH6 1st	455	TRN+I+G
RAG2 2nd	274	GTR+G
RAG2 3rd	273	K80+G
MYH6 2nd	181	HKY+I+G
MYH6 3rd	181	K80

References

1. Giuletta, A.M.; Pirani, J.R.; Harley, R.M. Espinhaço Range region, eastern Brazil. In *Centres of Plant Diversity: A Guide and Strategy for Their Conservation*; Davis, S.D., Heywood, V.H., Herrera-Macbryde, O., Villa-Lobos, J., Hamilton, A.C., Eds.; IUCN Publication Unit: Cambridge, UK, 1997; pp. 397–404.
2. Gonzaga, D.R.; Peixoto, A.L.; Neto, L.M. Patterns of richness and distribution of Cactaceae in the Serra da Mantiqueira, Southeast Brazil, and implications for its conservation. *Acta Bot. Bras.* **2018**, *33*, 97–105. [[CrossRef](#)]
3. Roxo, F.F.; Silva, G.S.C.; Zawadzki, C.H.; Oliveira, C. *Neoplecostomus doceensis*: A new loricariid species (Teleostei, Siluriformes) from the rio Doce basin and comments about its putative origin. *ZooKeys* **2014**, *440*, 115–127. [[CrossRef](#)] [[PubMed](#)]
4. De Medeiros, L.S.; Sarmiento-Soares, L.M.; Lima, S.M.Q. A new psammophilous catfish of the genus *Microcambeva* (Teleostei: Trichomycteridae) from the Rio Doce basin, southeastern Brazil. *Ichthyol. Explor. Freshw.* **2021**, *1147*, 1–13. [[CrossRef](#)]
5. Oliveira-Silva, L.; Santos, S.A.; Lopes, M.M.; Zanata, A.M. A new species of *Characidium* (Characiformes: Crenuchidae) from the rio Doce basin, Brazil. *Neotrop. Ichthyol.* **2022**, *20*, e210125. [[CrossRef](#)]
6. Reis, V.J.C.; de Pinna, M.C.C. Diversity and systematics of *Trichomycterus* Valenciennes 1832 (Siluriformes: Trichomycteridae) in the Rio Doce Basin: Iterating DNA, phylogeny and classical taxonomy. *Zool. J. Linn. Soc.* **2022**, *197*, 344–441. [[CrossRef](#)]
7. Alves, C.B.M.; Gomes, J.P.C.; Pessali, T.C.; Gasparini, J.L. Peixes ameaçados de extinção na bacia do Rio Doce. In *Livro Vermelho da Biota Aquática do Rio Doce Ameaçada de Extinção pós Rompimento da Barragem de Fundão, Mariana, Minas Gerais: Crustáceos, Efemerópteros, Odonatos e Peixes*; Drummond, G.M., Subira, R.J., Martins, C.S., Eds.; Fundação Biodiversitas: Belo Horizonte, Brazil, 2021; pp. 204–266.
8. Costa, W.J.E.M.; Katz, A.M. Integrative taxonomy supports high species diversity of south-eastern Brazilian mountain catfishes of the *T. reinhardti* group (Siluriformes: Trichomycteridae). *Syst. Biodivers.* **2021**, *19*, 601–621. [[CrossRef](#)]
9. Jankowsky, M.; de Carvalho, R.M.; do Patrocínio Gomes, V.A.; de Freitas, R.R. Peixes e pesca na bacia do Rio Doce, uma análise bibliométrica. *Brazil. J. Prod. Eng.* **2021**, *6*, 14–40. [[CrossRef](#)]
10. Costa, W.J.E.M. Comparative osteology, phylogeny and classification of the eastern South American catfish genus *Trichomycterus* (Siluriformes: Trichomycteridae). *Taxonomy* **2021**, *1*, 160–191. [[CrossRef](#)]
11. Katz, A.M.; Barbosa, M.A.; Mattos, J.L.O.; Costa, W.J.E.M. Multigene analysis of the catfish genus *Trichomycterus* and description of a new South American trichomycterine genus (Siluriformes, Trichomycteridae). *Zoosyst. Evol.* **2018**, *94*, 557–566. [[CrossRef](#)]
12. Costa, W.J.E.M.; Mattos, J.L.; Vilaro, P.J.; Amorim, P.F.; Katz, A.M. Perils of underestimating species diversity: Revisiting systematics of *Psammocambeva* catfishes (Siluriformes: Trichomycteridae) from the Rio Paraíba do Sul basin, south-eastern Brazil. *Taxonomy* **2022**, *2*, 491–523. [[CrossRef](#)]
13. Costa, W.J.E.M.; Azevedo-Santos, V.M.; Mattos, J.L.O.; Katz, A.M. Molecular phylogeny, taxonomy and distribution patterns of trichomycterine catfishes in the middle Rio Grande drainage, south-eastern Brazil (Siluriformes: Trichomycteridae). *Fishes* **2023**, *8*, 206. [[CrossRef](#)]
14. Vilaro, P.J.; Katz, A.M.; Costa, W.J.E.M. Phylogeny and historical biogeography of neotropical catfishes *Trichomycterus* (Siluriformes: Trichomycteridae) from eastern Brazil. *Mol. Phylog. Evol.* **2023**, *186*, 107836. [[CrossRef](#)] [[PubMed](#)]
15. Eigenmann, C.H. The localities at which Mr. John D. Haseman made collections. *Ann. Carnegie Mus.* **1911**, *7*, 299–314.
16. Eigenmann, C.H. Descriptions of sixteen new species of Pygidiidae. *Proc. Am. Philos. Soc.* **1917**, *56*, 690–703.
17. Eigenmann, C.H. The Pygidiidae, a family of South American catfishes. *Mem. Carnegie Mus.* **1918**, *7*, 259–398. [[CrossRef](#)]
18. Reis, V.J.C.; de Pinna, M.C.C.; Pessali, T.C. A new species of *Trichomycterus* Valenciennes, 1832 (Trichomycteridae: Siluriformes) from the Rio Doce drainage with remarkable similarities with *Bullockia* and a CT-scan survey. *J. Fish Biol.* **2020**, *95*, 918–931. [[CrossRef](#)]
19. Leary, S.; Underwood, W.; Anthony, R.; Cartner, S.; Corey, D.; Grandin, T.; Greenacre, C.; Gwaltney-Brant, S.; McCrackin, M.; Meyer, R.; et al. AVMA Guidelines for the Euthanasia of Animals: 2020 Edition. 2020. Available online: <http://www.avma.org/sites/default/files/2020-02/Guidelines-on-Euthanasia-2020.pdf> (accessed on 3 December 2022).
20. Taylor, W.R.; Van Dyke, G.C. Revised procedures for staining and clearing small fishes and other vertebrates for bone and cartilage study. *Cybium* **1985**, *9*, 107–119.
21. Costa, W.J.E.M. Description de huit nouvelles espèces du genre *Trichomycterus* (Siluriformes: Trichomycteridae), du Brésil oriental. *Rev. Française d'Aquariologie Herpétologie* **1992**, *18*, 101–110.
22. Costa, W.J.E.M.; Katz, A.M.; Mattos, J.L.O.; Amorim, P.F.; Mesquita, B.O.; Vilaro, P.J.; Barbosa, M.A. Historical review and redescription of three poorly known species of the catfish genus *Trichomycterus* from south-eastern Brazil (Siluriformes: Trichomycteridae). *J. Nat. Hist.* **2020**, *53*, 2905–2928. [[CrossRef](#)]
23. Bockmann, F.A.; Sazima, I. *Trichomycterus maracaya*, a new catfish from the upper rio Paraná, southeastern Brazil (Siluriformes: Trichomycteridae), with notes on the *T. brasiliensis* species-complex. *Neotrop. Ichthyol.* **2004**, *2*, 61–74. [[CrossRef](#)]
24. Kubicek, K.M. Developmental osteology of *Ictalurus punctatus* and *Noturus gyrinus* (Siluriformes: Ictaluridae) with a discussion of siluriform bone homologies. *Verteb. Zool.* **2022**, *72*, 661–727. [[CrossRef](#)]
25. Arratia, G.; Huaquin, L. Morphology of the lateral line system and of the skin of diplomystid and certain primitive loricarioid catfishes and systematic and ecological considerations. *Bonn Zool. Monogr.* **1995**, *36*, 1–110.
26. Villa-Verde, L.; Lazzarotto, H.; Lima, S.Q.M. A new glanapterygine catfish of the genus *Listrura* (Siluriformes: Trichomycteridae) from southeastern Brazil, corroborated by morphological and molecular data. *Neotrop. Ichthyol.* **2012**, *10*, 527–538. [[CrossRef](#)]

27. Ward, R.D.; Zemlak, T.S.; Innes, B.H.; Last, P.R.; Hebert, P.D. DNA barcoding Australia's fish species. *Philos. Trans. R. Soc. Lond. B Biol. Sci.* **2005**, *360*, 1847–1857. [[CrossRef](#)] [[PubMed](#)]
28. Palumbi, S.; Martin, A.P.; Romano, S.; McMillan, W.O.; Stice, L.; Grabowski, G. *The Simple Fool's Guide to PCR: Version 2.0*; University of Hawaii Press: Honolulu, HI, USA, 1991; 94p.
29. Costa, W.J.E.M.; Henschel, E.; Katz, A.M. Multigene phylogeny reveals convergent evolution in small interstitial catfishes from the Amazon and Atlantic forests (Siluriformes: Trichomycteridae). *Zool. Scr.* **2020**, *49*, 159–173. [[CrossRef](#)]
30. Tamura, K.; Stecher, G.; Kumar, S. MEGA11: Molecular Evolutionary Genetics Analysis Version 11. *Mol. Biol. Evol.* **2021**, *38*, 3022–3027. [[CrossRef](#)]
31. Chenna, R.; Sugawara, H.; Koike, T.; Lopez, R.; Gibson, T.J.; Higgins, D.G.; Thompson, J.D. Multiple sequence alignment with the Clustal series of programs. *Nucleic Acids Res.* **2003**, *31*, 3497–3500. [[CrossRef](#)]
32. Lanfear, R.; Frandsen, P.B.; Wright, A.M.; Senfeld, T.; Calcott, B. PartitionFinder 2: New methods for selecting partitioned models of evolution for molecular and morphological phylogenetic analyses. *Mol. Biol. Evol.* **2017**, *34*, 772–773. [[CrossRef](#)]
33. Ronquist, F.; Teslenko, M.; van der Mark, P.; Ayres, D.L.; Darling, A.; Höhna, S.; Larget, B.; Liu, L.; Suchard, M.A.; Huelsenbeck, J.P. MRBAYES 3.2: Efficient Bayesian phylogenetic inference and model selection across a large model space. *Syst. Biol.* **2012**, *61*, 539–542. [[CrossRef](#)]
34. Rambaut, A.; Drummond, A.J.; Xie, D.; Baele, G.; Suchard, M.A. Posterior summarisation in Bayesian phylogenetics using Tracer 1.7. *Syst. Biol.* **2018**, *67*, 901–904. [[CrossRef](#)]
35. Zwickl, D.J. Genetic Algorithm Approaches for the Phylogenetic Analysis of Large Biological Sequence Datasets under the Maximum Likelihood Criterion. Ph.D. Thesis, The University of Texas, Austin, TX, USA, 2006.
36. Felsenstein, J. Confidence limits on phylogenies: An approach using the bootstrap. *Evolution* **1985**, *39*, 783–791. [[CrossRef](#)]
37. Sarmiento-Soares, L.M.; Martins-Pinheiro, R.F.; Casagrande, M.D. Endemicity Analysis of the Ichthyofauna of the Rio Doce Basin, Southeastern Brazil. *Na. Acad. Bras. Cienc.* **2022**, *94*, e20210646. [[CrossRef](#)] [[PubMed](#)]
38. Feio, R.; Assis, C.; Lessa, G.; Ribon, R. *Fauna da Serra do Brigadeiro, Minas Gerais*; Universidade Federal de Viçosa: Viçosa, Brazil, 2019; 57p.
39. Lezama, A.Q.; Triques, M.L.; Santos, P.S. *Trichomycterus argos* (Teleostei: Siluriformes: Trichomycteridae), a new species from the Doce River Basin, Eastern Brazil. *Zootaxa* **2012**, *3352*, 60–68. [[CrossRef](#)]
40. Moreira, M.M.; Carrijo, T.T.; Alves-Araújo, A.G.; Rapini, A.; Salino, A.; Firmino, A.D.; Chagas, A.P.; Versiane, A.F.A.; Amorim, A.M.A.; da Silva, A.V.S.; et al. A list of land plants of Parque Nacional do Caparaó, Brazil, highlights the presence of sampling gaps within this protected area. *Biodivers. Data J.* **2020**, *8*, e59664. [[CrossRef](#)] [[PubMed](#)]
41. Zornosa-Torres, C.; Augusto-Alves, G.; Lyra, M.L.; Silva Júnior, J.C.; Garcia, P.C.A.; Leite, F.; Verdade, V.; Rodrigues, M.T.; Gasparini, J.L.; Haddad, C.F.B.; et al. Anurans of the Caparaó National Park and surroundings, southeast Brazil. *Biota Neotrop.* **2006**, *20*, e20190882. [[CrossRef](#)]
42. Rodrigues, M.T.; Cassimiro, J.; Pavan, D.; Curcio, F.F.; Verdade, V.K.; Pellegrino, K.C.M. A new genus of microteiid lizard from the Caparaó Mountains, Southeastern Brazil, with a discussion of relationships among Gymnophthalminae (Squamata). *Am. Mus. Novit.* **2009**, *3673*, 1–27. [[CrossRef](#)]
43. Alencar, A.R.; Costa, W.J.E.M. Description of two new species of the catfish genus *Trichomycterus* from southeastern Brazil (Siluriformes: Trichomycteridae). *Zootaxa* **2004**, *744*, 1–8. [[CrossRef](#)]
44. Barbosa, M.A.; Costa, W.J.E.M. Seven new species of the catfish genus *Trichomycterus* (Teleostei: Siluriformes: Trichomycteridae) from southeastern Brazil and re-description of *T. brasiliensis*. *Ichthyol. Explor. Freshw.* **2010**, *21*, 97–122.
45. Boulenger, G.A. Description of a new siluroid fish from the Organ Mountains, Brazil. *Ann. Mag. Nat. Hist. Ser. 6* **1896**, *18*, 154. [[CrossRef](#)]
46. Miranda Ribeiro, A. Vertebrados do Itatiaya (Peixes, Serpentes, Saurios, Aves e Mammíferos), resultados de excursões do Sr. Carlos Moreira, Assistente da Seção de Zoologia do Museu Nacional. *Arq. Mus. Nac.* **1906**, *13*, 165–190.
47. Miranda Ribeiro, P. Duas novas espécies de peixes na coleção ictiológica do Museu Nacional (Pisces, Callichthyidae et Pygidiidae). *Rev. Brasil. Biol.* **1949**, *9*, 143–145.
48. Reis, V.J.C.; dos Santos, S.A.; Britto, M.R.; Volpi, T.A.; de Pinna, M.C.C. Iterative taxonomy reveals a new species of *Trichomycterus Valenciennes 1832* (Siluriformes, Trichomycteridae) widespread in Rio Doce Basin: A pseudocryptic of *T. immaculatus*. *J. Fish Biol.* **2020**, *97*, 1607–1623. [[CrossRef](#)] [[PubMed](#)]
49. Costa, W.J.E.M.; Katz, A.M. A new catfish of the genus *Trichomycterus* from the Rio Paraíba do Sul Basin, south-eastern Brazil, a supposedly migrating species (Siluriformes, Trichomycteridae). *Zoosyst. Evol.* **2022**, *98*, 13–21. [[CrossRef](#)]
50. Costa, W.J.E.M.; Mattos, J.L.O.; Lopes, S.; Amorim, P.F.; Katz, A.M. Integrative taxonomy, distribution and ontogenetic colouration change in Neotropical mountain catfishes of the *Trichomycterus nigroauratus* group (Siluriformes: Trichomycteridae). *Zool. Stud.* **2022**, *61*, 11. [[CrossRef](#)]
51. Myers, N.; Mittermeir, R.A.; Mittermeir, C.G.; da Fonseca, G.A.B.; Kent, J. Biodiversity hotspots for conservation priorities. *Nature* **2000**, *403*, 853–858. [[CrossRef](#)]
52. Tamura, K.; Nei, M. Estimation of the number of nucleotide substitutions in the control region of mitochondrial DNA in humans and chimpanzees. *Mol. Biol. Evol.* **1993**, *10*, 512–526. [[CrossRef](#)]
53. Hasegawa, M.; Kishini, H.; Yano, T. Dating of the human-ape splitting by a molecular clock of mitochondrial DNA. *J. Mol. Evol.* **1985**, *22*, 160–174. [[CrossRef](#)] [[PubMed](#)]

54. Rodríguez, F.; Oliver, J.L.; Marín, A.; Medina, J.R. The general stochastic model of nucleotide substitution. *J. Theor. Biol.* **1990**, *22*, 485–501. [[CrossRef](#)]
55. Zharkikh, A. Estimation of evolutionary distances between nucleotide sequences. *J. Mol. Evol.* **1994**, *39*, 315–329. [[CrossRef](#)]
56. Kimura, M. A simple method for estimating evolutionary rates of base substitutions through comparative studies of nucleotide sequences. *J. Mol. Evol.* **1980**, *16*, 111–120. [[CrossRef](#)]

Disclaimer/Publisher’s Note: The statements, opinions and data contained in all publications are solely those of the individual author(s) and contributor(s) and not of MDPI and/or the editor(s). MDPI and/or the editor(s) disclaim responsibility for any injury to people or property resulting from any ideas, methods, instructions or products referred to in the content.